

PRODUCTION OF EXOTIC ATOMS

by

MARK ELLERMANN II

Submitted to the Faculty of the Graduate School
of Texas A&M University-Commerce
in partial fulfillment of the requirements
for the degree of
MASTER OF SCIENCE
December 2010

PRODUCTION OF EXOTIC ATOMS

Approved:

Adviser

Dean of the College of Arts & Science

Dean of Graduate Studies and Research

ABSTRACT

PRODUCTION OF EXOTIC ATOMS

Mark Ellermann, MS
Texas A&M University-Commerce, 2010

Adviser: Carlos Bertulani, PhD

I study in detail the space-time dependence of the production of muonic, pionic, and other exotic atoms by the coherent photon exchange between nuclei at the Large Hadron Collider (LHC) at the European Laboratory for Particle Physics (CERN). I show that a multipole expansion of the electromagnetic interaction yields an useful insight of the bound-free production mechanism which has not been explored in the literature. Predictions for the spatial, temporal, and angular distribution, as well as the total cross sections for the production of exotic atoms, are also included.

Acknowledgements

First I would like to thank my professor and thesis adviser, Dr. Carlos Bertulani, for the incredible support and advice he has given me both in class and out, as well as his companionship, which he offers to all students. I would also like to thank Dr. Li and Dr. Montgomery for giving their time to be on my thesis committee. To continue, I would like to thank Dr. Chourasia and Dr. Rogers for their teaching and support during my graduate work at Texas A&M University-Commerce. I especially want to thank my wife, Michal, who has given me constant support in my studies, and my parents, Mark and Lisa, for their support and constant encouragement to excel. Finally, I would like to thank my extended family, who have always supported me in my endeavors.

Table of Contents

1	INTRODUCTION	1
2	ELECTROMAGNETIC INTERACTION	4
2.1	The Lienard-Wiechert Potential	4
2.2	Hamiltonian for the Electromagnetic Interaction	9
2.3	Derivation of the relativistic Coulomb interactions	12
2.3.1	Electric dipole	13
2.3.2	Electric quadrupole	15
2.3.3	Magnetic dipole	17
2.3.4	Summary	18
2.4	Magnetic Interaction Between Particles	19
2.4.1	Non-relativistic expression	19
3	ANTI-HYDROGEN FORMATION	22
3.1	Introduction to Anti-Hydrogen Formation	22
3.2	Production of $\bar{\text{H}}$ with antiproton beams	23
3.3	Production of $\bar{\text{H}}$ by real photons	29
3.4	Production of $\bar{\text{H}}$ by virtual photons	34
3.5	The equivalent photon approximation	38
4	PRODUCTION OF EXOTIC ATOMS AT CERN LARGE HADRON COLLIDER	42
4.1	Production of exotic atoms in ion-ion collisions	42
4.2	Results	49

4.3 Conclusions	56
A POSITRON WAVEFUNCTION	62
B ELECTRON WAVEFUNCTION	66
C PLANE-WAVE BORN APPROXIMATION	68

List of Tables

- 4.1 Cross sections for production of exotic atoms in pp and Pb-Pb collisions at the CERN Large Hadron Collider (LHC). 56

List of Figures

2.1	Coordinates used to obtain eq. (2.44).	19
3.1	\bar{H} in collisions of \bar{p} with a nuclear target.	24
3.2	Angular distribution of electrons in \bar{H} production by real photons	30
3.3	Production cross sections by longitudinal and transverse virtual photons. Cross sections are calculated for $\varepsilon = 2$ and $\gamma = 3$	34
3.4	Production cross sections by longitudinal and transverse virtual photons. Cross sections are calculated for $\varepsilon = 2$ and $\gamma = 10$	35
3.5	\bar{H} production in collision of an antiproton with a proton target as a function of γ	36
3.6	\bar{H} production in collision of an antiproton with a proton target using a plane wave function for the electron and a hydrogenic wave function for \bar{H}	37
3.7	Virtual photon cross section for $\varepsilon = 1, 5,$ and $10,$ for $\gamma = 100,$ and as a function of q_t	38
3.8	Ratio between $\sigma_{\gamma^*t}(q_t = 0, \omega)$ and $\sigma_\gamma(\omega)$ for $\varepsilon = 1, 5,$ and $10,$ as a function of γ	39
3.9	Energy spectrum of the electron $\frac{d\sigma}{d\varepsilon}$ for $\gamma = 3, 10,$ and $100,$ respectively, from numerical integration of Eq. 3.32	40

- 4.1 Relative probability $P_{E\lambda}(b, t)/P_{E1}(b, t = \infty)$, for production of a muonic atom in pp collisions at the LHC with an impact parameter $b = a_{muon} = 255$ fm, where a_{muon} is the Bohr radius for a muonic atom. 49
- 4.2 Left: Coordinate distribution in the plane along the beam axis of the probability for production of muonic atoms with capture in the K-shell with pp collisions at the LHC. The impact parameter is chosen as $b = a_{muon} = 255$ fm and is along the vertical axis. Right: Same as the previous figure, but in the plane perpendicular to the beam axis. The impact parameter vector lies along the x direction. . . 52
- 4.3 Probability of muonic atom production in pp collisions at the LHC as a function of the impact parameter. 54
- 4.4 Contour plot with the angular distribution of the positive muon when the negative muon is captured by a proton at the LHC, as a function of the angle that the free muon has with the direction of motion of the muonic atom and of the energy of the free positive muon. 55

Chapter1

INTRODUCTION

It is undeniable that ultra-peripheral collisions (collisions dominated by the electromagnetic interaction) between relativistic heavy ions allows interesting physics to be probed. As far back as 1989 it was noticed that the Higgs boson could be produced at comparable rates as in central collisions between relativistic heavy ions [1, 2], the advantage being that ultra-peripheral collisions are cleaner in the sense that nothing else than the Higgs boson would be observed. By now, ultra-peripheral collisions are known as an excellent tool for several interesting phenomena and have been discussed in numerous publications, reviews, and popular articles (see, e.g. [3, 4]).

A process of interest in ultra-peripheral collisions with relativistic heavy ions is the production of pairs in which one of the particles is captured in an orbit around one of the ions in the collider (what is called “bound-free” pair production). In particular the process of pair-production with capture was used as a tool to generate the first artificial anti-hydrogen atom in the laboratory [5]. The pioneer CERN experiment was followed by another experiment at Fermilab [6]. The number of anti-atoms produced was shown to be in good agreement with detailed theoretical predictions [7].

I extend these studies by considering the production of exotic atoms in pp and heavy ion collisions such as those being carried out at the Large Hadron Collider (LHC) at CERN. In my notation, an exotic atom is an atom in which one electron has been replaced by other particles of the same charge. In contrast to previous approaches, I show that a multipole expansion of the electromagnetic field yields several insights in the production mechanism which have not been explored in the literature. My calculations apply to the production of muonic atoms, pionic atoms, protonium, etc. The Bohr radius for a muonic atom is much closer to the nucleus than in an ordinary atom, and corrections due to quantum electrodynamics are important. The energy levels and transition rates from excited states to the ground state of muonic atoms also provide experimental tests of quantum electrodynamics. Hadronic atoms, such as pionic hydrogen and kaonic hydrogen, also provide interesting experimental probes of the theory of quantum chromodynamics. A protonium is antiprotonic hydrogen, a composite of a negatively charged antiproton paired with a positively charged proton or nucleus. Protonium has been studied theoretically mainly by using non-relativistic quantum mechanics, which yields predictions for its binding energy and lifetime. The lifetimes are predicted in the range of 0.1-10 microseconds. While protonium production has a very small cross section in pp collisions at CERN, the cross section is appreciable

for heavy ions, e.g. for Pb-Pb collisions. In this case, the anti-proton will be captured in an orbit around one of the Pb nuclei. Such a system would be of large interest for understanding inter-nucleon forces in charge-conjugate channels.

Most of my calculations will be for the production of muonic atoms and pp collisions. There is no qualitative difference for the production of other exotic atoms via the same mechanism, except for the obvious reduction of the production yields due to mass differences. The production cross sections for Pb-Pb collisions will be enhanced by a large amount, approximately equal to $10^{10} - 10^{12}$, but the details of the production mechanism are essentially the same as in pp collisions.

In Chapter 2 I will discuss electromagnetic interactions between two relativistic ions. In Chapter 3 I will discuss the formation of Anti-Hydrogen and how it pertains to the production of exotic atoms, and in Chapter 4 I will discuss the theoretical production of exotic atoms. The Appendix contains explanatory derivations of some equations used in Chapter 3.

Chapter2

ELECTROMAGNETIC INTERACTION

2.1 The Lienard-Wiechert Potential

If a charge e is moving with a velocity \mathbf{v} within a Lorentz frame, S , we can transform the coordinates to a frame S' where the charge is seen as standing still. The S' frame moves with velocity \mathbf{v} with respect to the S frame of reference. For convenience, we can center the S' origin on the moving charge.

Now, in the S' frame, we can describe the electric potential as

$$\phi' = \frac{e}{r'}, \quad \mathbf{A}' = 0 \quad (2.1)$$

(All prime notations will refer to the quantity in the S' frame of reference)

As A^μ is a 4-vector, the components of A^μ transform according to Lorentz boosts just as the components of x^μ do. Therefore

$$\phi' = \gamma(\phi - \mathbf{v} \cdot \mathbf{A}) \quad (2.2)$$

and

$$\mathbf{A}' = \mathbf{A} + (\gamma - 1)\mathbf{v}v^2, \quad (2.3)$$

where $\gamma = (1 - v^2)^{-1/2}$. From the definitions we have set for the system, the Lorentz transformation is obtained by sending $\mathbf{v} \longrightarrow -\mathbf{v}$, thus

$$\phi = \gamma\phi' = \frac{e\gamma}{r'}, \quad \mathbf{A} = \mathbf{A}' + \frac{\gamma - 1}{v^2(\mathbf{v} \cdot \mathbf{A}')} \mathbf{v} + \gamma\mathbf{v}\phi' \quad (2.4)$$

From (2.4), we find the potentials in frame S , in which the particle is moving with velocity, \mathbf{v} , are given by

$$\phi = \gamma\phi' = \frac{e\gamma}{r'}, \quad \mathbf{A} = \gamma\mathbf{v}\phi' = \frac{e\gamma\mathbf{v}}{r'} \quad (2.5)$$

Here r' still appears in the denominator, and now we perform the transformation from primed to unprimed coordinate frames. Suppose the axes are aligned so that \mathbf{v} lies in the x direction. Then

$$x' = \gamma(x - vt), \quad y' = y, \quad z' = z, \quad (2.6)$$

and

$$r'^2 = x'^2 + y'^2 + z'^2 = \gamma^2(x - vt)^2 + y^2 + z^2 \quad (2.7)$$

It can now be seen that the scalar and 3-vector potentials in the S frame are

$$\phi = e/R_*, \quad \text{and} \quad \mathbf{A} = e\mathbf{v}/R_* \quad (2.8)$$

where

$$R_*^2 = (x - vt)^2 + (1 - v^2)(y^2 + z^2) \quad (2.9)$$

Now the electric and magnetic fields can be calculated from ϕ and \mathbf{A} . Alternatively, we can calculate \mathbf{E}' and \mathbf{B}' in the S' frame, and then transform them back to the unprimed frame. In S' we have

$$\mathbf{E}' = e\mathbf{r}'/r'^3, \quad \mathbf{B}' = 0 \quad (2.10)$$

To transform back to the unprimed frame, we can invert the results that express \mathbf{E}' and \mathbf{B}' in terms of \mathbf{E} and \mathbf{B} . Again, we can simply change \mathbf{v} to $-\mathbf{v}$, giving

$$\mathbf{E} = \gamma(\mathbf{E}' - \mathbf{v} \times \mathbf{B}') - \frac{\gamma - 1}{v^2}(\mathbf{v} \cdot \mathbf{E}')\mathbf{v} \quad (2.11)$$

$$\mathbf{B} = \gamma(\mathbf{B}' + \mathbf{v} \times \mathbf{E}') - \frac{\gamma - 1}{v^2}(\mathbf{v} \cdot \mathbf{B}')\mathbf{v} \quad (2.12)$$

so we find that \mathbf{E} and \mathbf{B} in the unprimed frame are ultimately given by

$$\mathbf{E} = \frac{e\gamma\mathbf{r}'}{r'^3} - \frac{\gamma - 1}{v^2} \frac{e\mathbf{v} \cdot \mathbf{r}'}{r'^3} \mathbf{v} \quad (2.13)$$

$$\mathbf{B} = \gamma\mathbf{v} \times \mathbf{E}' = \frac{e\gamma\mathbf{v} \times \mathbf{r}'}{r'^3} \quad (2.14)$$

Maintaining the orientation of the axes so that \mathbf{v} lies along the x -direction, we have

$$E_x = \frac{ex'}{r'^3}, \quad E_y = \frac{e\gamma y'}{r'^3}, \quad E_z = \frac{e\gamma z'}{r'^3} \quad (2.15)$$

converting to unprimed coordinates,

$$E_x = \frac{e\gamma(x - vt)}{r'^3}, \quad E_y = \frac{e\gamma y}{r'^3}, \quad E_z = \frac{e\gamma z}{r'^3} \quad (2.16)$$

To find the distance vector from the charge to the point $\mathbf{r} = (x, y, z)$, we recall the charge is located at $(vt, 0, 0)$ in the S frame, we have

$$\mathbf{R} = ((x - vt), y, z) \quad (2.17)$$

Combining this with (2.16), we then have

$$\mathbf{E} = \frac{e\gamma\mathbf{R}}{r'^3} = \frac{e(1 - v^2)\mathbf{R}}{R_*^3} \quad (2.18)$$

where R_* is defined by (2.8). With θ being defined as the angle between \mathbf{R} and the x-axis, the transformation of coordinates for the observation point is

$$y^2 + z^2 = R^2 \sin^2 \theta, \quad \text{where} \quad R^2 = |\mathbf{R}|^2 = (x - vt)^2 + y^2 + z^2 \quad (2.19)$$

Now it follows that

$$R_*^2 = R^2 - v^2(y^2 + z^2) = R^2(1 - v^2 \sin^2 \theta) \quad (2.20)$$

and substituting into (2.18)

$$\mathbf{E} = \frac{e\mathbf{R}}{R^3} \frac{1 - v^2}{(1 - v^2 \sin^2 \theta)^{3/2}} \quad (2.21)$$

Dividing this equation into its parallel and perpendicular components by setting $\theta = 0$ and $\pi/2$, we arrive at

$$\mathbf{E}_{\parallel} = \frac{e(1-v^2)}{R^2} \quad \text{and} \quad \mathbf{E}_{\perp} = \frac{e(1-v^2)^{-1/2}}{R^2} \quad (2.22)$$

As v approaches 1 (speed of light) \mathbf{E}_{\parallel} reduces to zero, and \mathbf{E}_{\perp} diverges, thus \mathbf{E} peaks at $\theta = \frac{\pi}{2}$. If we define γ

$$\gamma = \frac{\pi}{2} - \theta \quad (2.23)$$

then

$$|\mathbf{E}| = \frac{e(1-v^2)}{R^2(1-v^2\cos^2\gamma)^{3/2}} \quad (2.24)$$

and

$$|\mathbf{E}| \approx \frac{e(1-v^2)}{(1-v^2 + \frac{1}{2}\gamma^2)^{3/2}} \quad (2.25)$$

if $v \approx 1$. This leaves the angular width of the peak of the order of $\sqrt{1-v^2}$. Using (2.14) and the above result for \mathbf{E} we have

$$\mathbf{B} = \frac{e(1-v^2)\mathbf{v} \times \mathbf{R}}{R_*^3} \quad (2.26)$$

Checking consistency with established theory, if $|\mathbf{v}| \ll 1$, we again have the non-relativistic expressions for \mathbf{E} and \mathbf{B}

$$\mathbf{E} \approx \frac{e\mathbf{R}}{R^3}, \quad \mathbf{B} \approx \frac{e\mathbf{v} \times \mathbf{R}}{R^3} \quad (2.27)$$

2.2 Hamiltonian for the Electromagnetic Interaction

Using the homogeneous Maxwell equations we can write \mathbf{E} and \mathbf{B} in terms of auxiliary fields ϕ and \mathbf{A} , where ϕ is the electrostatic potential, and \mathbf{A} is the vector potential. Using this, \mathbf{E} and \mathbf{B} become

$$\mathbf{E} = -\nabla\phi - \frac{1}{c}\frac{\partial\mathbf{A}}{\partial t} \quad \text{and} \quad \mathbf{B} = \nabla \times \mathbf{A}. \quad (2.28)$$

And we can define the four-potential as

$$(A^\alpha) = \begin{pmatrix} \phi \\ \mathbf{A} \end{pmatrix}. \quad (2.29)$$

The Lorentz force for a moving particle is now

$$\frac{d}{dt} \frac{m\mathbf{v}}{\sqrt{1-v^2/c^2}} = q(\mathbf{E} + \frac{\mathbf{v}}{c} \times \mathbf{B}). \quad (2.30)$$

Using the definition of the four-potential we have

$$\begin{aligned} \frac{d}{dt} \frac{m\mathbf{v}}{\sqrt{1-v^2/c^2}} &= q[-\nabla\phi - \frac{1}{c}\frac{\partial\mathbf{A}}{\partial t} + \frac{\mathbf{v}}{c} \cdot (\nabla \times \mathbf{A})] \\ &= \nabla(-q\phi + q\frac{\mathbf{v}}{c} \cdot \mathbf{A}) - \frac{q}{c}(\frac{\partial}{\partial t} + \mathbf{v} \cdot \nabla)\mathbf{A} \\ &= \nabla(-q\phi + q\frac{\mathbf{v}}{c} \cdot \mathbf{A}) - \frac{q}{c}\frac{d\mathbf{A}}{dt} \end{aligned} \quad (2.31)$$

where

$$\frac{d\mathbf{A}[\mathbf{r}(\mathbf{t}), t]}{dt} = (\frac{\partial}{\partial t} + \mathbf{v} \cdot \nabla)\mathbf{A}[\mathbf{r}(t), t]. \quad (2.32)$$

Eq. (2.31) can be rewritten as

$$\frac{d}{dt} \left(\frac{m\mathbf{v}}{\sqrt{1-v^2/c^2}} + \frac{q}{c} \mathbf{A} \right) + \nabla \left(q\phi - \frac{q}{c} \mathbf{v} \cdot \mathbf{A} \right) = \mathbf{0} \quad (2.33)$$

This has the form of the Euler-Lagrange equations, and the Lagrangian that reproduces Eq. (2.31) when replaced in (2.33) is

$$\mathcal{L}(\mathbf{r}, \mathbf{v}) = -mc^2 \sqrt{1-v^2/c^2} + \frac{q}{c} \mathbf{v} \cdot \mathbf{A}(\mathbf{r}, t) - q\phi(\mathbf{r}, t). \quad (2.34)$$

The momentum can be calculated from the Lagrangian using

$$\mathbf{p} = \nabla_{\mathbf{v}} \mathcal{L} = \frac{m\mathbf{v}}{\sqrt{1-v^2/c^2}} + \frac{q}{c} \mathbf{A}(\mathbf{r}, t) = \mathbf{P} + \frac{q}{c} \mathbf{A}(\mathbf{r}, t), \quad (2.35)$$

where

$$\mathbf{P} = \frac{m\mathbf{v}}{\sqrt{1-v^2/c^2}}. \quad (2.36)$$

is the kinetic momentum and $q\mathbf{A}/c$ is momentum carried by the EM field.

Using the Lagrangian-Hamiltonian conversion we have

$$H = \mathbf{p} \cdot \mathbf{v} - \mathcal{L} = \frac{mc^2}{\sqrt{1-v^2/c^2}} + q\phi. \quad (2.37)$$

Which can be rewritten as

$$H(\mathbf{r}, \mathbf{p}) = c \left[\left(\mathbf{p} - \frac{q}{c} \mathbf{A}(\mathbf{r}, t) \right)^2 + (mc)^2 \right]^{1/2} + q\phi(\mathbf{r}, t). \quad (2.38)$$

For non-relativistic particles,

$$|\mathbf{P}| = \left| \mathbf{p} - \frac{q}{c} \mathbf{A} \right| \ll mc \quad (2.39)$$

so that

$$H(\mathbf{r}, \mathbf{p}) = mc^2 + \frac{(\mathbf{p} - q\mathbf{A}/c)^2}{2m} + q\phi \quad (2.40)$$

The $(q\mathbf{A})^2/2mc^2$ term is relevant to processes where two photons are involved and can be ignored for our purposes. Thus we have

$$H_{int} = q\phi - \frac{q}{c} \mathbf{v} \cdot \mathbf{A} \quad (2.41)$$

where the rest mass and kinetic energy of the particle has been subtracted from (2.40).

For particle systems involving charge density, $\rho(\mathbf{r}, t)$, and current density $\mathbf{j}(\mathbf{r}, t)$, H_{int} can be generalized to

$$H_{int} = \int H_{int} d^3r = \int [\rho\phi - \frac{1}{c} \mathbf{j} \cdot \mathbf{A}] d^3r. \quad (2.42)$$

Although this has been obtained under approximations, it is valid in general. Hamiltonian density can then be written as

$$H_{int} = \frac{1}{c} J_\mu A^\mu \quad (2.43)$$

2.3 Derivation of the relativistic Coulomb interactions

We start with Eq.(2.15) of [8],

$$a_{i \rightarrow f} = -i \frac{Z_1 e^2}{\hbar v \gamma} \sum_{\pi \lambda \mu} G_{\pi \lambda \mu} \left(\frac{c}{v} \right) (-)^{\mu} K_{\mu} \left(\frac{\omega b}{v \gamma} \right) \hat{\lambda} \left(\frac{\omega}{c} \right)^{\lambda} \mathcal{M}_{\pi \lambda, -\mu} / e,$$

$$\mathcal{M}_{\pi \lambda, -\mu} = \langle I_f M_f | M(\pi, \lambda, -\mu) | I_i M_i \rangle,$$

where b is the impact parameter and K_{μ} is the modified Bessel function of 2nd kind and $\hat{\lambda} = \sqrt{2\lambda + 1}$. We define the following form of the Coulomb interaction with multipole decomposition:

$$V_{\pi \lambda \mu}^{i \rightarrow f}(t) = \frac{i \hbar}{2\pi} \frac{[\int_{-\infty}^{\infty} a_{i \rightarrow f}(\omega) e^{-i\omega t} d\omega]_{\pi \lambda \mu}}{\mathcal{M}_{\pi \lambda, -\mu}}.$$

Then we find

$$\begin{aligned} V_{\pi \lambda \mu}^{i \rightarrow f}(t) &= \frac{Z_1 e}{2\pi v \gamma} G_{\pi \lambda \mu} \left(\frac{c}{v} \right) \int_{-\infty}^{\infty} (-)^{\mu} K_{\mu} \left(\frac{\omega b}{v \gamma} \right) \hat{\lambda} \left(\frac{\omega}{c} \right)^{\lambda} e^{-i\omega t} d\omega \\ &\equiv \frac{Z_1 e}{2\pi v \gamma} G_{\pi \lambda \mu} \left(\frac{c}{v} \right) \hat{\lambda} I_{\lambda \mu}(t). \end{aligned}$$

Using the following properties of K_{μ} ,

$$K_{\mu}(-x) = (-)^{\mu} K_{\mu}(x)$$

and

$$K_{-\mu}(x) = K_{\mu}(x),$$

the integral $I_{\lambda\mu}(t)$ can be written as

$$\begin{aligned}
I_{\lambda\mu}(t) &\equiv \int_{-\infty}^{\infty} (-)^{\mu} K_{\mu} \left(\frac{\omega b}{v\gamma} \right) \left(\frac{\omega}{c} \right)^{\lambda} e^{-i\omega t} d\omega \\
&= \int_{-\infty}^0 (-)^{\mu} K_{\mu} \left(\frac{\omega b}{v\gamma} \right) \left(\frac{\omega}{c} \right)^{\lambda} e^{-i\omega t} d\omega + \int_0^{\infty} (-)^{\mu} K_{\mu} \left(\frac{\omega b}{v\gamma} \right) \left(\frac{\omega}{c} \right)^{\lambda} e^{-i\omega t} d\omega \\
&= - \int_0^{\infty} (-)^{\mu} K_{\mu} \left(\frac{-\omega' b}{v\gamma} \right) \left(\frac{-\omega'}{c} \right)^{\lambda} e^{i\omega' t} d\omega' \\
&\quad + \int_0^{\infty} (-)^{\mu} K_{\mu} \left(\frac{\omega b}{v\gamma} \right) \left(\frac{\omega}{c} \right)^{\lambda} e^{-i\omega t} d\omega \\
&= \int_0^{\infty} (-)^{\lambda} K_{\mu} \left(\frac{\omega' b}{v\gamma} \right) \left(\frac{\omega'}{c} \right)^{\lambda} e^{i\omega' t} d\omega' + \int_0^{\infty} (-)^{\mu} K_{\mu} \left(\frac{\omega b}{v\gamma} \right) \left(\frac{\omega}{c} \right)^{\lambda} e^{-i\omega t} d\omega \\
&= \int_0^{\infty} K_{\mu} \left(\frac{\omega b}{v\gamma} \right) \left(\frac{\omega}{c} \right)^{\lambda} \left\{ (-)^{\lambda} e^{i\omega t} + (-)^{\mu} e^{-i\omega t} \right\} d\omega.
\end{aligned}$$

Using this expression we find also

$$\begin{aligned}
I_{\lambda, -\mu}(t) &= \int_{-\infty}^{\infty} K_{-\mu} \left(\frac{\omega b}{v\gamma} \right) \left(\frac{\omega}{c} \right)^{\lambda} \left\{ (-)^{\lambda} e^{i\omega t} + (-)^{-\mu} e^{-i\omega t} \right\} d\omega \\
&= \int_0^{\infty} K_{\mu} \left(\frac{\omega b}{v\gamma} \right) \left(\frac{\omega}{c} \right)^{\lambda} \left\{ (-)^{\lambda} e^{i\omega t} + (-)^{\mu} e^{-i\omega t} \right\} d\omega \\
&= I_{\lambda\mu}(t),
\end{aligned}$$

since μ is an integer.

In the following we calculate each component of $I_{\lambda\mu}(t)$ for the electric dipole ($\lambda = 1$) and quadrupole ($\lambda = 2$) excitation potentials, assuming $t > 0$.

2.3.1 Electric dipole

I_{11} :

$$I_{11}(t) = \int_0^{\infty} K_1 \left(\frac{\omega b}{v\gamma} \right) \left(\frac{\omega}{c} \right) \left\{ -e^{i\omega t} - e^{-i\omega t} \right\} d\omega = -\frac{2}{c} \int_0^{\infty} K_1 \left(\frac{\omega b}{v\gamma} \right) \omega \cos(\omega t) d\omega.$$

Using the integration formula

$$\int_0^{\infty} K_1 \left(\frac{\omega b}{v\gamma} \right) \omega \cos(\omega t) d\omega = \frac{\pi b}{2 v\gamma} \frac{1}{\left\{ \left(\frac{b}{v\gamma} \right)^2 + t^2 \right\}^{3/2}},$$

we obtain

$$\begin{aligned} I_{11}(t) &= -\frac{2\pi b}{c} \frac{1}{2 v\gamma \left\{ \left(\frac{b}{v\gamma} \right)^2 + t^2 \right\}^{3/2}} = -\frac{\pi b}{c v\gamma} \frac{v^3 \gamma^3}{(b^2 + v^2 \gamma^2 t^2)^{3/2}} \\ &= -\frac{\pi v^2 \gamma^2}{c} \frac{b}{(b^2 + v^2 \gamma^2 t^2)^{3/2}}. \end{aligned}$$

I_{10} :

$$\begin{aligned} I_{10}(t) &= \int_{-2i}^{\infty} K_0 \left(\frac{\omega b}{v\gamma} \right) \left(\frac{\omega}{c} \right) \{-e^{i\omega t} + e^{-i\omega t}\} d\omega = \frac{-2i}{c} \int_0^{\infty} K_1 \left(\frac{\omega b}{v\gamma} \right) \omega \sin(\omega t) d\omega \\ &= \frac{-2i}{c} \frac{1}{2 \left\{ 1 + \left(\frac{b}{v\gamma t} \right)^2 \right\}^{3/2} t^2} = \frac{-i\pi v^2 \gamma^2}{c} \frac{1}{(b^2 + v^2 \gamma^2 t^2)^{3/2}}. \end{aligned}$$

Using the following form of $G_{E1\mu}$ given in Appendix B of Winther and Alder,

$$G_{E11}(x) = \frac{1}{3} \sqrt{8\pi} x = -G_{E1,-1}(x), \quad G_{E10}(x) = -i \frac{4}{3} \sqrt{\pi} (x^2 - 1)^{1/2},$$

we have

$$\begin{aligned} V_{E11}^{i \rightarrow f}(t) &= \frac{Z_1 e}{2\pi v\gamma} G_{E11} \left(\frac{c}{v} \right) \sqrt{3} I_{11}(t) = -\frac{Z_1 e}{2\pi v\gamma} \frac{1}{3} \sqrt{8\pi} \frac{c}{v} \sqrt{3} \frac{\pi v^2 \gamma^2}{c} \frac{b}{(b^2 + v^2 \gamma^2 t^2)^{3/2}} \\ &= -\sqrt{\frac{2\pi}{3}} Z_1 e \gamma \frac{b}{(b^2 + v^2 \gamma^2 t^2)^{3/2}}, \end{aligned}$$

$$\begin{aligned}
V_{E10}^{i \rightarrow f}(t) &= \frac{Z_1 e}{2\pi v \gamma} G_{E10} \left(\frac{c}{v} \right) \sqrt{3} I_{10}(t) \\
&= \frac{Z_1 e}{2\pi v \gamma} i \frac{4}{3} \sqrt{\pi} \left\{ \left(\frac{c}{v} \right)^2 - 1 \right\}^{1/2} \sqrt{3} \frac{i\pi v^2 \gamma^2}{c} \frac{v \gamma t}{(b^2 + v^2 \gamma^2 t^2)^{3/2}} \\
&= -\sqrt{\frac{4\pi}{3}} Z_1 e \frac{c}{v} \left\{ 1 - \left(\frac{v}{c} \right)^2 \right\}^{1/2} \frac{v \gamma}{c} \frac{v \gamma t}{(b^2 + v^2 \gamma^2 t^2)^{3/2}} \\
&= -\sqrt{\frac{4\pi}{3}} Z_1 e \frac{c}{v \gamma} \frac{v \gamma}{c} \frac{v \gamma t}{(b^2 + v^2 \gamma^2 t^2)^{3/2}} \\
&= -\sqrt{\frac{4\pi}{3}} Z_1 e \frac{v \gamma t}{(b^2 + v^2 \gamma^2 t^2)^{3/2}},
\end{aligned}$$

$$V_{E1,-1}^{i \rightarrow f}(t) = -V_{E11}^{i \rightarrow f}(t).$$

2.3.2 Electric quadrupole

I_{22} :

$$\begin{aligned}
I_{22}(t) &= \int_{-\infty}^{\infty} K_2 \left(\frac{\omega b}{v \gamma} \right) \left(\frac{\omega}{c} \right)^2 \left\{ (-)^2 e^{i\omega t} + (-)^2 e^{-i\omega t} \right\} d\omega \\
&= \frac{2}{c^2} \int_0^{\infty} K_2 \left(\frac{\omega b}{v \gamma} \right) \omega^2 \cos(\omega t) d\omega \\
&= \frac{2}{c^2} \frac{3\pi}{2} \left(\frac{b}{v \gamma} \right) \frac{1}{\left\{ \left(\frac{b}{v \gamma} \right)^2 + t^2 \right\}^{5/2}} = \frac{3\pi v^3 \gamma^3}{c^2} \frac{b^2}{(b^2 + v^2 \gamma^2 t^2)^{5/2}}.
\end{aligned}$$

I_{21} :

$$\begin{aligned}
I_{21}(t) &= \int_{-\infty}^{\infty} K_1 \left(\frac{\omega b}{v \gamma} \right) \left(\frac{\omega}{c} \right)^2 \left\{ (-)^2 e^{i\omega t} + (-)^1 e^{-i\omega t} \right\} d\omega \\
&= \frac{2i}{c^2} \int_0^{\infty} K_1 \left(\frac{\omega b}{v \gamma} \right) \omega^2 \sin(\omega t) d\omega \\
&= \frac{2i}{c^2} \frac{3\pi}{2} \left(\frac{b}{v \gamma} \right) \frac{1}{\left\{ 1 + \left(\frac{b}{v \gamma t} \right)^2 \right\}^{5/2}} \frac{1}{t^4} = \frac{3\pi i v^3 \gamma^3}{c^2} \frac{b v \gamma t}{(b^2 + v^2 \gamma^2 t^2)^{5/2}}.
\end{aligned}$$

I_{20} :

$$\begin{aligned}
I_{20}(t) &= \int_0^\infty K_0\left(\frac{\omega b}{v\gamma}\right) \left(\frac{\omega}{c}\right)^2 \left\{(-)^2 e^{i\omega t} + (-)^0 e^{-i\omega t}\right\} d\omega \\
&= \frac{2}{c^2} \int_0^\infty K_0\left(\frac{\omega b}{v\gamma}\right) \omega^2 \cos(\omega t) d\omega \\
&= \frac{2\pi}{c^2} \frac{\left(\frac{b}{v\gamma}\right)^2 - 2t^2}{2 \left\{\left(\frac{b}{v\gamma}\right)^2 + t^2\right\}^{5/2}} = \frac{\pi v^3 \gamma^3}{c^2} \frac{(b^2 - 2v^2 \gamma^2 t^2)}{(b^2 + v^2 \gamma^2 t^2)^{5/2}}.
\end{aligned}$$

Using

$$G_{E22}(x) = -\frac{2}{5} \sqrt{\frac{\pi}{6}} x (x^2 - 1)^{1/2} = G_{E2,-2}(x),$$

$$G_{E21}(x) = i \frac{2}{5} \sqrt{\frac{\pi}{6}} (2x^2 - 1) = i G_{E2,-1}(x),$$

$$G_{E20}(x) = \frac{2}{5} \sqrt{\pi} x (x^2 - 1)^{1/2},$$

we find

$$\begin{aligned}
V_{E22}^{i \rightarrow f}(t) &= \frac{Z_1 e}{2\pi v \gamma} G_{E22}\left(\frac{c}{v}\right) \sqrt{5} I_{22}(t) \\
&= -\frac{Z_1 e}{2\pi v \gamma} \frac{2}{5} \sqrt{\frac{\pi}{6}} \frac{c}{v} \left\{\left(\frac{c}{v}\right)^2 - 1\right\}^{1/2} \sqrt{5} \frac{3\pi v^3 \gamma^3}{c^2} \frac{b^2}{(b^2 + v^2 \gamma^2 t^2)^{5/2}} \\
&= -Z_1 e \sqrt{\frac{3\pi}{10}} \frac{\gamma b^2}{(b^2 + v^2 \gamma^2 t^2)^{5/2}},
\end{aligned}$$

$$\begin{aligned}
V_{E21}^{i \rightarrow f}(t) &= \frac{Z_1 e}{2\pi v \gamma} G_{E21} \left(\frac{c}{v} \right) \sqrt{5} I_{21}(t) \\
&= \frac{Z_1 e}{2\pi v \gamma} i \frac{2}{5} \sqrt{\frac{\pi}{6}} \left(2 \left(\frac{c}{v} \right)^2 - 1 \right) \sqrt{5} \frac{3\pi i v^3 \gamma^3}{c^2} \frac{b v \gamma t}{(b^2 + v^2 \gamma^2 t^2)^{5/2}} \\
&= -Z_1 e \sqrt{\frac{3\pi}{10}} \left(2 \left(\frac{c}{v} \right)^2 - 1 \right) \frac{v^2}{c^2} \frac{v \gamma^3 b t}{(b^2 + v^2 \gamma^2 t^2)^{5/2}} \\
&= -Z_1 e \sqrt{\frac{3\pi}{10}} \left(2 - \frac{v^2}{c^2} \right) \frac{\gamma^3 b v t}{(b^2 + v^2 \gamma^2 t^2)^{5/2}},
\end{aligned}$$

$$\begin{aligned}
V_{E20}^{i \rightarrow f}(t) &= \frac{Z_1 e}{2\pi v \gamma} G_{E20} \left(\frac{c}{v} \right) \sqrt{5} I_{20}(t) \\
&= \frac{Z_1 e}{2\pi v \gamma} \frac{2}{5} \sqrt{\pi} \frac{c}{v} \left\{ \left(\frac{c}{v} \right)^2 - 1 \right\}^{1/2} \sqrt{5} \frac{\pi v^3 \gamma^3}{c^2} \frac{(b^2 - 2v^2 \gamma^2 t^2)}{(b^2 + v^2 \gamma^2 t^2)^{5/2}} \\
&= Z_1 e \sqrt{\frac{\pi}{5}} \gamma \frac{(b^2 - 2v^2 \gamma^2 t^2)}{(b^2 + v^2 \gamma^2 t^2)^{5/2}},
\end{aligned}$$

$$V_{E2,-1}^{i \rightarrow f}(t) = -V_{E21}^{i \rightarrow f}(t),$$

$$V_{E2,-2}^{i \rightarrow f}(t) = V_{E22}^{i \rightarrow f}(t).$$

2.3.3 Magnetic dipole

For the magnetic dipole excitations the integrals are the same as for the E1 case, but

$$G_{M11}(x) = -i \frac{1}{3} \sqrt{8\pi} = G_{M1,-1}(x), \quad G_{M10}(x) = 0,$$

We have

$$\begin{aligned}
V_{M11}^{i \rightarrow f}(t) &= \frac{Z_1 e}{2\pi v \gamma} G_{M11} \left(\frac{c}{v} \right) \sqrt{3} I_{11}(t) = i \frac{Z_1 e}{2\pi v \gamma} \frac{1}{3} \sqrt{8\pi} \sqrt{3} \frac{\pi v^2 \gamma^2}{c} \frac{b}{(b^2 + v^2 \gamma^2 t^2)^{3/2}} \\
&= i \sqrt{\frac{2\pi}{3}} Z_1 e \frac{v}{c} \gamma \frac{b}{(b^2 + v^2 \gamma^2 t^2)^{3/2}},
\end{aligned}$$

$$V_{M10}^{i \rightarrow f}(t) = 0,$$

$$V_{M1,-1}^{i \rightarrow f}(t) = V_{M11}^{i \rightarrow f}(t).$$

2.3.4 Summary

In conclusion, we have shown

$$V_{E1\mu}^{i \rightarrow f}(t) = \sqrt{\frac{2\pi}{3}} \frac{Z_1 e \gamma}{(b^2 + v^2 \gamma^2 t^2)^{3/2}} \begin{cases} \mp b & \text{if } \mu = \pm 1 \\ \sqrt{2} vt & \text{if } \mu = 0 \end{cases}$$

$$V_{E2\mu}^{i \rightarrow f}(t) = \sqrt{\frac{3\pi}{10}} \frac{Z_1 e \gamma}{(b^2 + v^2 \gamma^2 t^2)^{5/2}} \begin{cases} b^2 & \text{if } \mu = \pm 2 \\ \mp \left(2 - \frac{v^2}{c^2}\right) \gamma^2 b v t & \text{if } \mu = \pm 1 \\ \sqrt{\frac{2}{3}} (b^2 - 2v^2 \gamma^2 t^2) & \text{if } \mu = 0 \end{cases}$$

In addition, we have

$$V_{M1\mu}^{i \rightarrow f}(t) = i \sqrt{\frac{2\pi}{3}} \frac{v}{c} \frac{Z_1 e \gamma}{(b^2 + v^2 \gamma^2 t^2)^{3/2}} \begin{cases} \pm b & \text{if } \mu = \pm 1 \\ 0 & \text{if } \mu = 0 \end{cases}$$

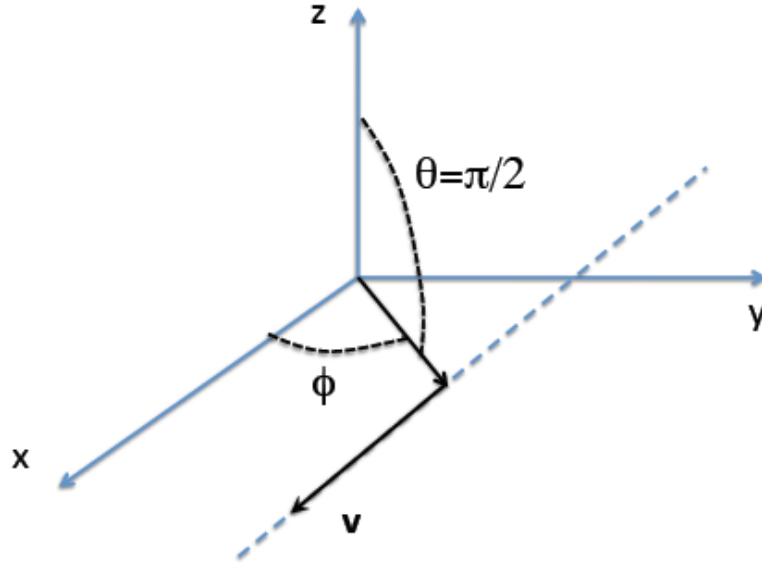


Figure 2.1: Coordinates used to obtain eq. (2.44).

2.4 Magnetic Interaction Between Particles

2.4.1 Non-relativistic expression

We start with Eq.(II.2.16) of [8] for M1 magnetic excitations:

$$V(t) = \frac{4\pi}{3} Z_p e \sum_{\mu} (-1)^{\mu} S_{1\mu}(t) \mathcal{M}_{1\mu}(\mathbf{r}) \quad (2.44)$$

where

$$\mathcal{M}_{1\mu} = -\frac{i}{2c} r (\mathbf{j}(\mathbf{r}) \cdot \mathbf{L}) Y_{1\mu}(\hat{\mathbf{r}}) \quad (2.45)$$

is the intrinsic M1 operator and the orbital integral is given by

$$S_{1\mu}(t) = \frac{i}{c r^2(t)} (\mathbf{v} \cdot \mathbf{L}) Y_{1\mu}(\theta(t), \phi(t)) \quad (2.46)$$

This result is obtained in the frame of reference shown by figure 4.4, with $\theta(t) = \pi/2$.

In order to obtain the expression in the frame of reference with the velocity along the z-axis, we have to rotate this expression to the new frame, remembering that the orbital integrals rotate as spherical tensors. One immediate observation is that the operator $\mathbf{v} \cdot \mathbf{L}$ is a scalar and therefore in the new system it will be given by vL_z . Using $L_z Y_{1\nu} = \nu Y_{1\nu}$, the expression for the M1 potential in the new frame is

$$V_{M1\mu}(t) = i \frac{4\pi}{3} Z_p e \frac{v}{c} \frac{1}{r^2(t)} (-1)^\mu \mu \mathcal{M}_{1\mu}(\mathbf{r}) \sum_{\nu} \mathcal{D}_{\mu\nu}^1 \left(-\frac{\pi}{2}, \frac{\pi}{2}, \frac{\pi}{2} \right) \nu Y_{1\nu} \left(\frac{\pi}{2}, \phi(t) \right). \quad (2.47)$$

Using

$$\mathcal{D}_{\mu\nu}^1 \left(-\frac{\pi}{2}, \frac{\pi}{2}, \frac{\pi}{2} \right) = \exp \left(i \frac{\pi}{2} \mu \right) d_{\mu\nu}^1 \left(\frac{\pi}{2} \right) \exp \left(-i \frac{\pi}{2} \nu \right) = i^{\mu-\nu} d_{\mu\nu}^1 \left(\frac{\pi}{2} \right)$$

and

$$d_{11}^1 \left(\frac{\pi}{2} \right) = d_{1,-1}^1 \left(\frac{\pi}{2} \right) = d_{-1,1}^1 \left(\frac{\pi}{2} \right) = d_{-1,-1}^1 \left(\frac{\pi}{2} \right) = \frac{1}{2}, \quad d_{10}^1 \left(\frac{\pi}{2} \right) = -\frac{1}{\sqrt{2}},$$

we get

$$V_{M1\mu}(t) = \frac{2\pi}{3} Z_p e \frac{v}{c} \frac{1}{r^2(t)} (-1)^\mu \mu \mathcal{M}_{1\mu}(\mathbf{r}) \left[Y_{1,-1} \left(\frac{\pi}{2}, \phi(t) \right) + Y_{11} \left(\frac{\pi}{2}, \phi(t) \right) \right]. \quad (2.48)$$

But

$$Y_{1,\pm 1} = \mp \frac{1}{2} \sqrt{\frac{3}{2\pi}} \exp(\pm i\phi)$$

and

$$\begin{aligned} V_{M1\mu}(t) &= -i \sqrt{\frac{2\pi}{3}} Z_p e^{-\frac{v}{c} r(t)} (-1)^\mu \mu \mathcal{M}_{1\mu}(\mathbf{r}) \sin \phi(t). \\ &= i \sqrt{\frac{2\pi}{3}} Z_p e^{-\frac{v}{c} r(t)} \mu \mathcal{M}_{1\mu}(\mathbf{r}) \frac{b}{r(t)} \\ &= i \sqrt{\frac{2\pi}{3}} Z_p e^{-\frac{v}{c} r(t)} \mu \mathcal{M}_{1\mu}(\mathbf{r}) \frac{b}{(b^2 + v^2 t^2)^{3/2}} \end{aligned} \quad (2.49)$$

Chapter 3

ANTI-HYDROGEN FORMATION

3.1 Introduction to Anti-Hydrogen Formation

Antihydrogen in flight was first produced and detected at CERN/LEAR [5] using the process

$$\bar{p} + Z \longrightarrow \bar{H} + e^{-} + Z, \quad (3.1)$$

where $Z=54$ (Xe). This process was first suggested by Munger et al. [10], where also calculations of the cross section for the antihydrogen production were performed in the equivalent photon approximation (EPA). A similar pair production process with e-capture will occur with large cross section at relativistic heavy ion colliders [4]. This is important because it leads to a beam loss. Theoretical calculations were done by many groups [11, 12, 13]. They were mainly interested in the limit of high energies. The applicability of EPA will become more and more questionable for the lower energies, where the \bar{H} production experiments were done [9, 14]. The dominant graph is shown in figure 1. It was shown in [14] that bremsstrahlung pair production with capture can be safely neglected.

By crossing symmetry the process $\gamma + \bar{p} \longrightarrow e^{-} + \bar{H}$ [10] is related to the photoeffect $\gamma + H \longrightarrow p + e^{-}$ [11] which is treated in the literature (see e.g. [15]). These calculations provide approximate theoretical values

for the $\bar{\text{H}}$ production cross section. This is also relevant for the ongoing experiments at Fermilab [16], where also the energy dependence of the process will be investigated and possible future experiments with fast $\bar{\text{H}}$ beams, like Lamb shift measurements [10, 16].

3.2 Production of $\bar{\text{H}}$ with antiproton beams

In the semiclassical approach we assume that the relativistic antiproton moves along a straight line. In its frame of reference the time-dependent electromagnetic fields of the target nucleus is given by

$$\mathbf{A}(\mathbf{r}, t) = \mathbf{v} \phi(\mathbf{r}, t), \quad \text{where} \quad \phi(\mathbf{r}, t) = \frac{Z_T e}{|\mathbf{r} - \mathbf{r}'(t)|}, \quad (3.2)$$

where $\mathbf{r} = (x, y, z)$, and $\mathbf{r}' = (b_x, b_y, \gamma vt)$, where v is the relative velocity, $\gamma = (1 - v^2)^{-1/2}$, and $Z_T e$ is the target charge. We can write ϕ in the integral representation

$$\phi(\mathbf{r}, t) = \frac{Z_T e}{2\pi^2} \int d^3q \frac{e^{i\mathbf{q} \cdot [\mathbf{r} - \mathbf{r}'(t)]}}{q^2}. \quad (3.3)$$

In the first-order perturbation theory, the $\bar{\text{H}}$ -production amplitude for a collision with impact parameter $b = \sqrt{b_x^2 + b_y^2}$ is given in terms of the transition density and current, $\rho(\mathbf{r})$ and $\mathbf{j}(\mathbf{r})$, respectively,

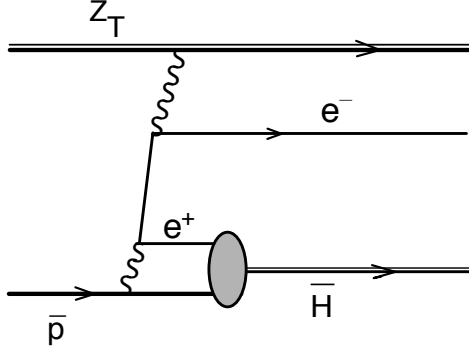


Figure 3.1: \bar{H} in collisions of \bar{p} with a nuclear target.

by

$$\begin{aligned}
 a_{1st} &= \frac{1}{i} \int dt e^{i\omega t} \int d^3r [\rho(\mathbf{r}) \phi(\mathbf{r}, t) - \mathbf{j}(\mathbf{r}) \cdot \mathbf{A}(\mathbf{r}, t)] \\
 &= \frac{Z_T e}{i\pi v} \int dt e^{i\omega t} \int d^3q \int d^3r \frac{e^{i\mathbf{q} \cdot [\mathbf{r} - \mathbf{r}'(t)]}}{q^2} [\rho(\mathbf{r}) - \mathbf{v} \cdot \mathbf{j}(\mathbf{r})] , \quad (3.4)
 \end{aligned}$$

where $\omega = \varepsilon + m$ is the sum of the electron, ε , and the positron energy, m (the binding energy of \bar{H} can be neglected). In the last step we have used eqs. 3.2 and 3.3. Performing the integral over time and using the continuity equation, $\nabla \cdot \mathbf{j} = -i\omega\rho$, we get

$$a_{1st} = \frac{Z_T e}{i\pi v} \int d^2q_t \frac{e^{i\mathbf{q}_t \cdot \mathbf{b}}}{Q^2} \int d^3r e^{i\mathbf{Q} \cdot \mathbf{r}} \left(\frac{j_z(\mathbf{r})}{v\gamma^2} + \frac{\mathbf{q}_t \cdot \mathbf{j}_t}{\omega} \right) , \quad (3.5)$$

where the index $z(t)$ denotes the components along (transverse to) the beam direction, and $\mathbf{Q} \equiv (\mathbf{q}_t, \omega/v)$. The transition current is given in terms of the Dirac matrices, $\vec{\alpha}$, and the lepton wavefunctions $\mathbf{j}(r) =$

$e [\Psi^{(-)}]^* \vec{\alpha} \Psi^{(+)}$. Thus we can rewrite the \bar{H} -production as

$$a_{1st} = \frac{Z_T e}{i\pi v} \int d^2 q_t \frac{e^{i\mathbf{q}_t \cdot \mathbf{b}}}{\left[q_t^2 + (\omega/\gamma v)^2 \right]^2} F(\mathbf{Q}) , \quad (3.6)$$

where

$$\begin{aligned} F(\mathbf{Q}) &= e \int d^3 r \left[\Psi^{(-)} \right]^* (\mathbf{r}) e^{i\mathbf{Q} \cdot \mathbf{r}} \left(\frac{\alpha_z}{v\gamma^2} + \frac{\mathbf{q}_t \cdot \vec{\alpha}_t}{\omega} \right) \Psi^{(+)}(\mathbf{r}) \\ &= ie \mathbf{K} \cdot \int d^3 r \left[\Psi^{(-)} \right]^* (\mathbf{r}) e^{i\mathbf{Q} \cdot \mathbf{r}} \gamma^0 \vec{\gamma} \Psi^{(+)}(\mathbf{r}) . \end{aligned} \quad (3.7)$$

In the last equality we used the definition $\mathbf{K} \equiv (\mathbf{K}_t, K_z) = (\mathbf{q}_t/\omega, 1/v\gamma^2)$ and $(\gamma^0, \vec{\gamma})$ are the Dirac matrices, where we follow the procedure of ref. [15]. The total cross section is obtained by integrating the square of the expression ?? over all possible impact parameters:

$$\sigma = \sum_{spins} \int |a_{1st}|^2 d^2 b = 4 \left(\frac{Z_T e}{v} \right)^2 \sum_{spins} \int_0^\infty d^2 q_t \frac{|F(\mathbf{Q})|^2}{(Q^2 - \omega^2)^2} . \quad (3.8)$$

The same result can be obtained in the Plane-Wave Born approximation, as shown in the appendix C. Using the positron and the electron wavefunctions as given by eqs. A.4 and eq. B.1 of the appendix, we

get

$$\begin{aligned}
F(\mathbf{Q}) &= ie \int d^3r \left\{ \bar{u} e^{-i\mathbf{p}\cdot\mathbf{r}} + \bar{\Psi}' \right\} (\vec{\gamma}\cdot\mathbf{K}) e^{i\mathbf{Q}\cdot\mathbf{r}} \\
&\times \left\{ 1 + \frac{i}{2m} \gamma^0 \vec{\gamma}\cdot\vec{\nabla} \right\} \mathbf{v}\Psi_{non-r}(\mathbf{r}) \\
&\simeq ie \int d^3r \left\{ \bar{u} e^{i(\mathbf{Q}-\mathbf{p})\cdot\mathbf{r}} (\vec{\gamma}\cdot\mathbf{K}) \left[\left(1 + \frac{i}{2m} \gamma^0 \vec{\gamma}\cdot\vec{\nabla} \right) \right] \mathbf{v}\Psi_{non-r}(\mathbf{r}) \right. \\
&+ \left. \bar{\Psi}' e^{i\mathbf{Q}\cdot\mathbf{r}} (\vec{\gamma}\cdot\mathbf{K}) \mathbf{v}\Psi_{non-r}(\mathbf{r}) \right\}, \tag{3.9}
\end{aligned}$$

where in the last equation we neglected terms of highest order in $Z\alpha$.

Integrating by parts

$$\begin{aligned}
F(\mathbf{Q}) &= ie \int d^3r \left\{ \bar{u} e^{i(\mathbf{Q}-\mathbf{p})\cdot\mathbf{r}} (\vec{\gamma}\cdot\mathbf{K}) \left[\left(1 + \frac{1}{2m} \gamma^0 \vec{\gamma}\cdot\vec{\nabla} \right) \mathbf{v}\Psi_{non-r}(\mathbf{r}) \right] \right. \\
&+ \left. \bar{\Psi}' e^{i\mathbf{Q}\cdot\mathbf{r}} (\vec{\gamma}\cdot\mathbf{K}) \mathbf{v}\Psi_{non-r}(\mathbf{r}) \right\} \\
&\simeq \frac{ie}{\sqrt{\pi}} a_0^{-3/2} \int d^3r \left\{ \bar{u} (\vec{\gamma}\cdot\mathbf{K}) \right. \\
&\times \left[\left(1 + \frac{1}{2m} \gamma^0 \vec{\gamma}\cdot(\mathbf{Q}-\mathbf{p}) \right) \mathbf{v} \left(e^{-r/a_0} \right)_{\mathbf{Q}-\mathbf{p}} \right] \\
&+ \left. \bar{\Psi}'_{\mathbf{Q}} (\vec{\gamma}\cdot\mathbf{K}) \mathbf{v} \right\}. \tag{3.10}
\end{aligned}$$

Since the corrections are in first order in $Z\alpha$, we have replaced $\Psi_{non-r}(\mathbf{r})$ by its constant value $1/\sqrt{\pi}a_0^{3/2}$ in the last term of the above equation. If we would do the same in the first term it would be identically zero (except for $\mathbf{Q} = \mathbf{p}$). This is the reason why we need to keep the corrections in the wavefunctions to first order in $Z\alpha$; for $\varepsilon \gg m$ these corrections yield a term of the same order as the plane-wave to the total cross section, as we shall see later. We rewrite the above

equation as

$$F(\mathbf{Q}) = 4ie\sqrt{\pi}a_0^{-5/2} \frac{\bar{u}Av}{(\mathbf{Q} - \mathbf{p})^2}, \quad (3.11)$$

where

$$A = a(\vec{\gamma} \cdot \mathbf{K}) + (\vec{\gamma} \cdot \mathbf{K})\gamma^0(\vec{\gamma} \cdot \mathbf{b}) + (\vec{\gamma} \cdot \mathbf{d})\gamma^0(\vec{\gamma} \cdot \mathbf{K}), \quad (3.12)$$

with

$$\begin{aligned} a &= \frac{1}{(\mathbf{Q} - \mathbf{p})^2} - \frac{\varepsilon}{Q^2 - p^2}, & \mathbf{b} &= \frac{\mathbf{Q} - \mathbf{p}}{2m(\mathbf{Q} - \mathbf{p})^2}, & \text{and} \\ \mathbf{c} &= -\frac{\mathbf{Q} - \mathbf{p}}{2m(Q^2 - p^2)}. \end{aligned} \quad (3.13)$$

Inserting 3.11 into 3.8, the cross section becomes

$$\sigma = \frac{16e^2}{\pi^2 a_0^5} \left(\frac{Z_T e}{v} \right)^2 \int \frac{d^3 p}{(2\pi)^3} \int_0^\infty \frac{d^2 q_t}{(Q^2 - \omega^2)^2} \frac{1}{(\mathbf{Q} - \mathbf{p})^4} \sum_{spins} |\bar{u}Av|^2. \quad (3.14)$$

The sum runs over the spins of the positron and the electron. Using $p^2 dp = \varepsilon p d\varepsilon$, and standard trace techniques we get

$$\begin{aligned} \frac{d\sigma}{d\varepsilon d\Omega} &= \frac{32e^2 p}{\pi^2 a_0^5} \left(\frac{Z_T e}{v} \right)^2 \int_0^\infty \frac{d^2 q_t}{(Q^2 - \omega^2)^2} \frac{1}{(\mathbf{Q} - \mathbf{p})^4} \\ &\times \left\{ (\varepsilon - 1) \left[(\mathbf{b} - \mathbf{d})^2 K^2 + 4(\mathbf{K} \cdot \mathbf{b})(\mathbf{K} \cdot \mathbf{d}) \right] \right. \\ &\left. + (\varepsilon + 1) a^2 K^2 + 2a \left[2(\mathbf{p} \cdot \mathbf{K})(\mathbf{b} \cdot \mathbf{K}) - \mathbf{p} \cdot (\mathbf{b} - \mathbf{d}) K^2 \right] \right\} \end{aligned} \quad (3.15)$$

Using the definition of \mathbf{K} , it is illustrative to separate the integrand of the above equation in terms of longitudinal and transverse components:

$$\frac{d\sigma}{d\varepsilon d\Omega} = \frac{1}{\pi\omega} \left(\frac{Z_T e}{v} \right)^2 \int_0^\infty d(q_t^2) \frac{q_t^2}{(Q^2 - \omega^2)^2} \times \left[\frac{d\sigma_{\gamma^*T}}{d\Omega}(\mathbf{Q}, \omega) + \frac{d\sigma_{\gamma^*L}}{d\Omega}(\mathbf{Q}, \omega) + \frac{d\sigma_{\gamma^*LT}}{d\Omega}(\mathbf{Q}, \omega) \right] \quad (3.16)$$

where

$$\begin{aligned} \frac{d\sigma_{\gamma^*T}}{d\Omega}(\mathbf{Q}, \omega) &= \frac{32e^2 p}{a_0^5 \omega} \frac{1}{(\mathbf{Q} - \mathbf{p})^4} \\ &\times \left\{ (\varepsilon - 1) \left[(\mathbf{b} - \mathbf{d})^2 - \frac{(q_t - \mathbf{p} \cdot \hat{\mathbf{e}}_t) \mathbf{p} \cdot \hat{\mathbf{e}}_t}{(\mathbf{Q} - \mathbf{p})^2 (Q^2 - p^2)} \right] \right. \\ &\left. + (\varepsilon + 1) a^2 + 2a \left[\frac{(q_t - \mathbf{p} \cdot \hat{\mathbf{e}}_t) \mathbf{p} \cdot \hat{\mathbf{e}}_t}{(\mathbf{Q} - \mathbf{p})^2} - \mathbf{p} \cdot (\mathbf{b} - \mathbf{d}) \right] \right\} \quad (3.17) \end{aligned}$$

$$\begin{aligned} \frac{d\sigma_{\gamma^*L}}{d\Omega}(\mathbf{Q}, \omega) &= \frac{32e^2 p \omega}{a_0^5 q_t^2} \left(\frac{1}{\gamma^2 v} \right)^2 \frac{1}{(\mathbf{Q} - \mathbf{p})^4} \\ &\times \left\{ (\varepsilon - 1) \left[(\mathbf{b} - \mathbf{d})^2 - \frac{(\omega/v - p_z)^2}{(\mathbf{Q} - \mathbf{p})^2 (Q^2 - p^2)} \right] \right. \\ &\left. + (\varepsilon + 1) a^2 + 2a \left[\frac{p_z (\omega/v - p_z)}{(\mathbf{Q} - \mathbf{p})^2} - \mathbf{p} \cdot (\mathbf{b} - \mathbf{d}) \right] \right\} \quad (3.18) \end{aligned}$$

$$\begin{aligned}
\frac{d\sigma_{\gamma^*LT}}{d\Omega}(\mathbf{Q}, \omega) &= \frac{64e^2p}{a_0^5 q_t \gamma^2 v} \frac{(\omega/v - p_z)}{(\mathbf{Q} - \mathbf{p})^6} \\
&\times \left\{ a \left[(\mathbf{p} \cdot \hat{\mathbf{e}}_t) + p_z \frac{(q_t - \mathbf{p} \cdot \hat{\mathbf{e}}_t)}{(\omega/v - p_z)} \right] \right. \\
&\left. - (\varepsilon - 1) \frac{(q_t - \mathbf{p} \cdot \hat{\mathbf{e}}_t)}{(Q^2 - p^2)} \right\} \quad (3.19)
\end{aligned}$$

In these equations $\hat{\mathbf{e}} = \hat{\mathbf{q}}_t/q_t$ is a unit vector in the transverse direction. The cross sections σ_{γ^*T} , σ_{γ^*L} , and σ_{γ^*LT} are interpreted as the cross sections for $\bar{\mathbb{H}}$ by virtual transverse and longitudinal photons and a interference term, respectively. Note that the transverse and longitudinal directions are *with respect to the beam axis*, nor with respect to the photon momentum, as is usually meant by this term. Only for $\gamma \gg 1$, this definition agrees with the definition of transverse and longitudinal virtual photons. However, this separation is very useful, as we will see next.

3.3 Production of $\bar{\mathbb{H}}$ by real photons

The cross section for production of $\bar{\mathbb{H}}$ by real photons is given by [15]

$$d\sigma_\gamma = 2\pi |V_{fi}|^2 \delta(\omega - \varepsilon - 1) \frac{d^3p}{(2\pi)^3}, \quad (3.20)$$

where

$$V_{fi} = -e \sqrt{\frac{4\pi}{\omega}} \int d^3r \left[\Psi^{(-)}(\mathbf{r}) \right]^* e^{i\mathbf{k} \cdot \mathbf{r}} (\hat{\mathbf{e}} \cdot \vec{\alpha}) \Psi^{(+)}(\mathbf{r}), \quad (3.21)$$

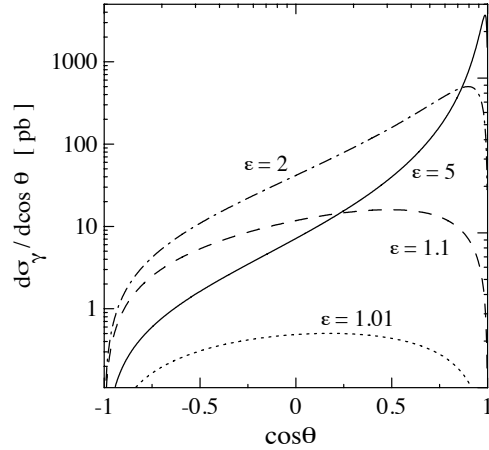


Figure 3.2: Angular distribution of electrons in \bar{H} production by real photons

with $\kappa = \hat{\mathbf{z}} \omega/c$, where $\hat{\mathbf{z}}$ is the unit vector along the photon incident direction, and $\hat{\mathbf{e}}$ is photon polarization unit vector. Using the positron and the electron wavefunctions as given by eqs. A.4 and eq. B.1 of the appendix, and performing similar steps as in section 3.2, we get

$$V_{fi} = -e \frac{8\pi\sqrt{2}}{a_0^{5/2}\omega^{1/2}} \frac{uBv}{(\kappa - \mathbf{p})^2}, \quad (3.22)$$

where

$$B = a_\kappa(\vec{\gamma} \cdot \vec{\kappa}) + (\vec{\gamma} \cdot \vec{\kappa})\gamma^0(\vec{\gamma} \cdot \mathbf{b}_\kappa) + (\vec{\gamma} \cdot \mathbf{d}_\kappa)\gamma^0(\vec{\gamma} \cdot \vec{\kappa}). \quad (3.23)$$

where a_κ , \mathbf{b}_κ , and \mathbf{d}_κ are the quantities defined in eqs. 3.13, but with \mathbf{Q} replaced by $\vec{\kappa} = \hat{\mathbf{z}} \omega/c$. Inserting these results in eq. 3.20 and summing over spins we get

$$\begin{aligned} \frac{d\sigma_\gamma}{d\Omega}(\omega) &= \frac{32e^2p}{a_0^5\omega} \frac{1}{(\kappa - \mathbf{p})^4} \\ &\times \left\{ (\varepsilon - 1) \left[(\mathbf{b}_\kappa - \mathbf{d}_\kappa)^2 - \frac{(\mathbf{p} \cdot \hat{\mathbf{e}})^2}{(\kappa - \mathbf{p})^2 (\kappa^2 - p^2)} \right] \right. \\ &+ \left. (\varepsilon + 1) a_\kappa^2 + 2a_\kappa \left[\frac{(\mathbf{p} \cdot \hat{\mathbf{e}})^2}{(\kappa - \mathbf{p})^2} - \mathbf{p} \cdot (\mathbf{b}_\kappa - \mathbf{d}_\kappa) \right] \right\}. \end{aligned} \quad (3.24)$$

We notice that the above equation can also be obtained from eqs. 3.16-3.19 in the limit $q_t \rightarrow 0$ and $v \rightarrow c$. In this limit $\sigma_{\gamma^*L} \rightarrow 0$, and $\sigma_{\gamma^*LT} \rightarrow 0$, and σ_{γ^*T} becomes the cross section for the production $\bar{\text{H}}$ by real photons.

Integrating eq. 3.24 over the azimuthal angle we get

$$\frac{d\sigma_\gamma}{d\theta}(\omega) = 2\pi \frac{e^2 p^3 (\varepsilon + 2)}{a_0^5 \omega^4} \frac{\sin^3 \theta}{(\varepsilon - p \cos \theta)^4} \left[\varepsilon - p \cos \theta - \frac{2}{\omega(\varepsilon + 2)} \right] \quad (3.25)$$

without any further approximations.

In figure 3.2 we plot the cross section for the angular distribution of the electrons in $\bar{\text{H}}$ production by real photons. We observe that the higher the electron energy is, the more forward peaked the distribution becomes. As we can immediately deduce from eq. 3.25, for $\varepsilon \gg 1$, the width of the peak is given by $\Delta \cos \theta \simeq 1$. For $\varepsilon \simeq 1$ the distribution is proportional to $\sin^2 \theta$. Integrating eq. 3.25 over θ we get

$$\sigma(\gamma + \bar{\text{p}} \rightarrow e^- + \bar{\text{H}}) = \frac{4\pi e^2}{a_0^5} \frac{p}{\omega^4} \left[\varepsilon^2 + \frac{2}{3}\varepsilon + \frac{4}{3} - \frac{\varepsilon + 2}{p} \ln(\varepsilon + p) \right] \quad (3.26)$$

It is instructive to derive this cross section by a different method. In some textbooks (see, e.g., ref. [15, 17]) one can find a calculation of the cross sections for the annihilation of a positron with an electron in the K-shell of a nucleus. From charge conjugation invariance (which is valid for QED), this cross section is the same as the cross section for the annihilation of an electron with a positron in the K-shell of an $\bar{\text{H}}$. The cross section is [17, 18]

$$\sigma(e^- + \bar{\text{H}} \rightarrow \gamma + \bar{\text{p}}) = \frac{2\pi e^2}{a_0^5} \frac{1}{p\omega^2} \left[\varepsilon^2 + \frac{2}{3}\varepsilon + \frac{4}{3} - \frac{\varepsilon + 2}{p} \ln(\varepsilon + p) \right] \quad (3.27)$$

Using the detailed balance theorem, the above equation yields exactly the same cross section of $\bar{\text{H}}$ production by real photons as given by eq. 3.26. The reason is that the calculation leading to eq. 3.26, originally due to Sauter [19], used the same corrections to $Z\alpha$ order for the electron and positron wavefunctions, as we did to obtain eq. 3.20(see Appendix).

The relevance of these corrections can be better understood by using the high energy limit, $\varepsilon \gg 1$. From eq. 3.26 we get

$$\sigma(\gamma + \bar{\text{p}} \rightarrow e^- + \bar{\text{H}}) = \frac{4\pi e^2}{a_0^5} \frac{1}{\varepsilon} \quad (3.28)$$

If in our calculation, we had used plane-waves for the electron and the hydrogenic wave function for the positron, without the corrections to

order $Z\alpha$, the cross section for the production of \bar{H} by real photons would be given by

$$\left[\frac{d\sigma_\gamma}{d\theta}(\omega) \right]_{PWA} = 4\pi \frac{e^2 p}{a_0^5 \omega^4} \frac{\sin \theta}{(\varepsilon - p \cos \theta)^4}, \quad (3.29)$$

the integral of which being

$$[\sigma_\gamma]_{PWA} = \frac{8\pi e^2}{a_0^5} \frac{p}{\omega^4} (3\varepsilon^2 + p^2). \quad (3.30)$$

In the high energy limit:

$$[\sigma_\gamma]_{PWA} = \frac{32\pi e^2}{3a_0^5} \frac{1}{\varepsilon} \quad (3.31)$$

We see that the difference between this result and that of eq. 3.28 is a factor $8/3$. This is just the reason why the corrections of order $Z\alpha$ have to be included in the calculation of \bar{H} . They yield terms to the matrix elements for photo-production of \bar{H} of the same order as the terms of lowest order. The origin of the difference between the two results are the small distances which enter in the calculation of the matrix elements of eq. 3.10. The corrections are essential to account for their effects properly. We note that these corrections are enough to account for a good description of \bar{H} production. photons and by virtual ones will prove to be very useful, as we shall see in the next section.

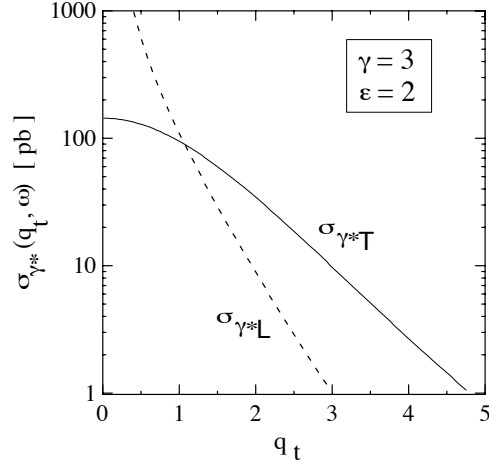


Figure 3.3: Production cross sections by longitudinal and transverse virtual photons. Cross sections are calculated for $\varepsilon = 2$ and $\gamma = 3$

3.4 Production of \bar{H} by virtual photons

As we have seen in last section, the production of \bar{H} in a collision of \bar{p} with nuclear targets is directly related to the production cross section by real photons in the limit $q_t \rightarrow 0$ and $v \rightarrow c$. It is important to determine at which values of q_t and γ this condition applies. In figures 3.3 and 3.4 we plot the production cross sections by longitudinal and transverse virtual photons, σ_{γ^*T} , σ_{γ^*L} , respectively. These are the integrals of eqs. 3.17 and 3.18, which are performed numerically. The integral of the interference term, σ_{γ^*LT} , eq. 3.19, is very small and is not shown. In figure 3.3 the cross sections are calculated for $\varepsilon = 2$, and $\gamma = 3$, and in figure 3.4 for $\gamma = 10$ and $\varepsilon = 2$. We observe that for low γ 's the cross section σ_{γ^*L} , is as important as σ_{γ^*T} , while for large γ 's the cross section σ_{γ^*T} dominates. For large γ 's the cross section σ_{γ^*L} is

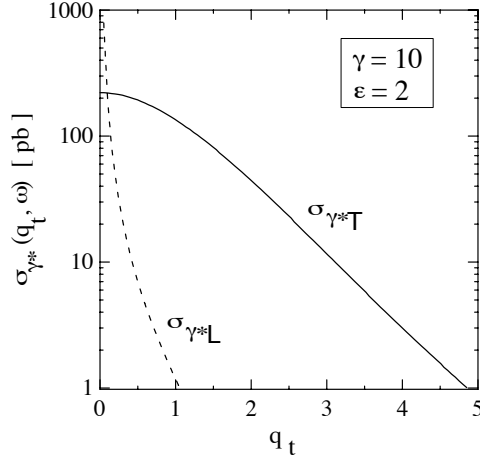


Figure 3.4: Production cross sections by longitudinal and transverse virtual photons. Cross sections are calculated for $\varepsilon = 2$ and $\gamma = 10$

only relevant at $q_t \simeq 0$. But this region contributes little to the total cross section, which is given by

$$\sigma = \frac{1}{\pi\omega} \left(\frac{Z_T e}{v} \right)^2 \int_1^\infty d\varepsilon \int_0^\infty d(q_t^2) \frac{q_t^2}{(Q^2 - \omega^2)^2} \times [\sigma_{\gamma^*T}(Q, \omega) + \sigma_{\gamma^*L}(Q, \omega) + \sigma_{\gamma^*L}(Q, \omega)] , \quad (3.32)$$

since the first term inside the integral suppresses $q_t \simeq 0$ values. This can also be seen by calculating the total cross section for \bar{H} production as a function of γ . This is shown in figure 3.5 where the solid curve shows the cross section as given by eq. 3.32, and the dashed line is the cross section with only the inclusion of σ_{γ^*T} . We see that for γ of the order of 8, or larger, the cross section is dominated by the transverse virtual photon component. Moreover we also observe that the cross section for large γ 's disagree with the equivalent photon approximation (EPA)

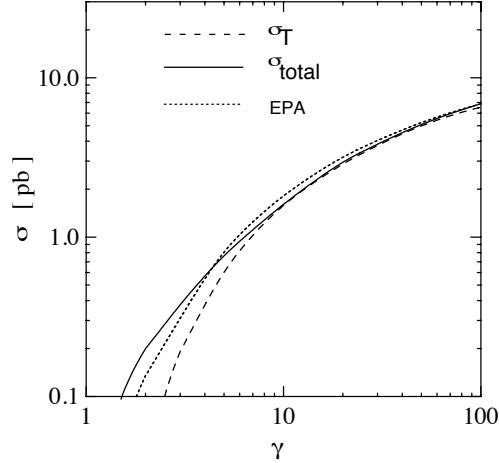


Figure 3.5: \bar{H} production in collision of an antiproton with a proton target as a function of γ .

used in ref. [10] to calculate the cross section for the production of \bar{H} . It is thus convenient to study under what circumstances the equivalent photon approximation is reliable.

It might appear strange that the longitudinal part of the cross section is relevant until such large values of γ . It is thus reasonable to check this result with a more schematic calculation. This can be achieved by using plane-waves for the electron and hydrogenic waves for the positron, without the correction terms to order $Z\alpha$. In this case, we get

$$F(\mathbf{Q}) = 4ie\sqrt{\pi}a_0^{-5/2} \frac{\bar{u}(\vec{\gamma} \cdot \mathbf{K})v}{(\mathbf{Q} - \mathbf{p})^2}, \quad (3.33)$$

which yields the cross section

$$\frac{d\sigma}{d\varepsilon d\Omega} = \frac{1}{\pi\omega} \left(\frac{Z_T e}{v} \right)^2 \int_0^\infty d(q_t^2) \frac{q_t^2}{(Q^2 - \omega^2)^2} \left[\frac{d\sigma_{\gamma^*T}}{d\Omega}(\mathbf{Q}, \omega) + \frac{d\sigma_{\gamma^*L}}{d\Omega}(\mathbf{Q}, \omega) \right], \quad (3.34)$$

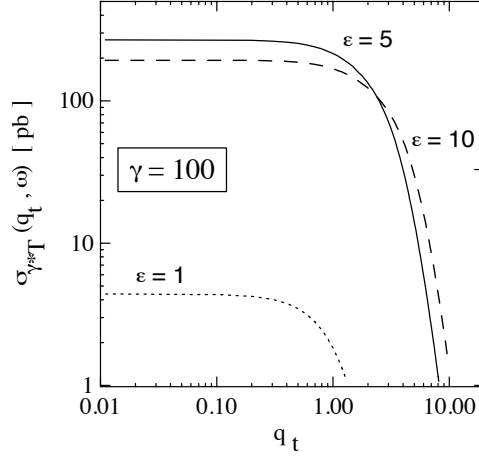


Figure 3.6: \bar{H} production in collision of an antiproton with a proton target using a plane wave function for the electron and a hydrogenic wave function for \bar{H}

where the interference term is exactly zero, and

$$\frac{d\sigma_{\gamma^*T}}{d\Omega}(\mathbf{Q}, \omega) = \frac{32e^2p}{a_0^5} \frac{1}{(\mathbf{Q} - \mathbf{p})^8} \quad (3.35)$$

and

$$\frac{d\sigma_{\gamma^*L}}{d\Omega}(\mathbf{Q}, \omega) = \frac{32e^2p\omega^2}{a_0^5q_t^2} \left(\frac{1}{\gamma^2v} \right)^2 \frac{1}{(\mathbf{Q} - \mathbf{p})^8}. \quad (3.36)$$

The integral over Ω in the expressions above can be done analytically yielding

$$\left\{ \begin{array}{l} \sigma_{\gamma^*T}(Q, \omega) \\ \sigma_{\gamma^*L}(Q, \omega) \end{array} \right\} = \frac{128\pi e^2p}{3a_0^5} \frac{(p^2 + 3Q^2)(3p^2 + Q^2)}{(Q^2 - p^2)^6} \left\{ \begin{array}{l} 1 \\ \omega^2/(q_t\gamma^2v)^2 \end{array} \right\}. \quad (3.37)$$

Using this result, the integral over q_t^2 in (4.3) can also be performed analytically but resulting in too long expressions to be transcribed here.

In figure 3.9 we plot $1 - (d\sigma_L/d\varepsilon)/(d\sigma_T/d\varepsilon)$ obtained in this approxi-

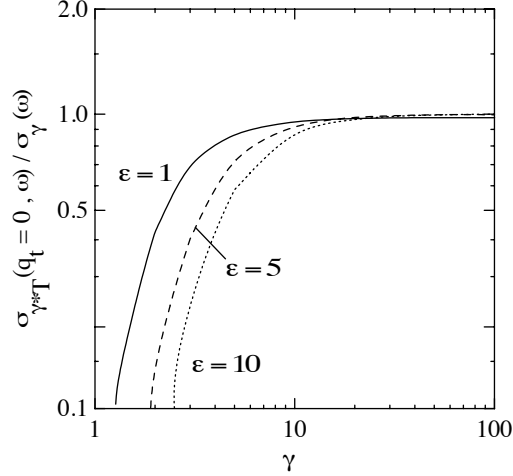


Figure 3.7: Virtual photon cross section for $\varepsilon = 1, 5$, and 10 , for $\gamma = 100$, and as a function of q_t .

mation, for $\varepsilon = 1, 2$, and 3 , respectively, and as a function of γ . We observe indeed that even for relatively large values of γ (e.g., $\gamma \sim 5$) the longitudinal part of the cross section is still substantially relevant for the calculation of the total cross section.

3.5 The equivalent photon approximation

The equivalent photon approximation is a well known method to obtain cross sections for virtual photon processes in QED. It is described in several textbooks (see, e.g., [15]). It is valid for large γ 's, in which case the cross section is dominated by transverse photons, as with the production cross section of \overline{H} . In figure 3.7 we plot the virtual photon cross section $\sigma_{\gamma^*T}(Q, \omega)$ for $\varepsilon = 1, 5$, and 10 , for $\gamma = 100$, and as a function of q_t . In this logarithmic plot it is evident that the function $\sigma_{\gamma^*T}(Q, \omega)$ is approximately constant until a cutoff value, q_t^{\max} , at which

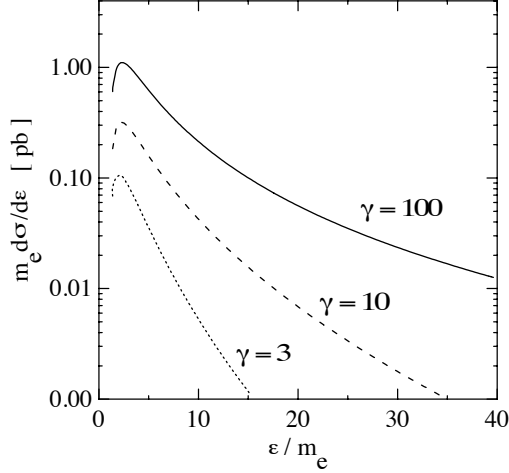


Figure 3.8: Ratio between $\sigma_{\gamma^*t}(q_t = 0, \omega)$ and $\sigma_\gamma(\omega)$ for $\varepsilon = 1, 5$, and 10 , as a function of γ

it drops rapidly to zero. On the other hand, the function

$$n(\gamma, Q) = \frac{1}{\pi} \left(\frac{Z_T e}{v} \right)^2 \frac{q_t^2}{(Q^2 - \omega^2)^2} \quad (3.38)$$

which we call by “equivalent photon number”, is strongly peaked at $q_t \simeq \omega/\gamma v$, which is very small for $\gamma \gg 1$. Thus it is fair to write

$$\begin{aligned} \frac{d\sigma}{d\varepsilon} &= \int_0^{q_t^{\max}} d(q_t^2) \frac{1}{\omega} n(\gamma, Q) \sigma_{\gamma^*T}(q_t = 0, \omega) \\ &\simeq \frac{1}{\omega} \sigma_\gamma(\omega) \int_0^{q_t^{\max}} d(q_t^2) n(\gamma, Q) \end{aligned} \quad (3.39)$$

where in the last equality we have approximated $\sigma_{\gamma^*T}(q_t = 0, \omega) \simeq \sigma_\gamma(\omega)$. This approximation is indeed valid for $\gamma \gg 1$, as we can see from figure 3.8, where we plot the ratio between these two quantities for $\varepsilon = 1, 5$, and 10 , and as a function of γ . For γ bigger than 10 the approximation is quite good, and it is even better for the lower values

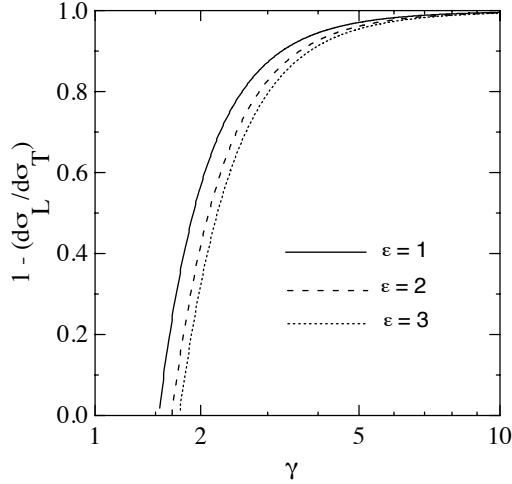


Figure 3.9: Energy spectrum of the electron $\frac{d\sigma}{d\varepsilon}$ for $\gamma = 3, 10,$ and $100,$ respectively, from numerical integration of Eq. 3.32

of ε . Eq. 3.39 is known as the “equivalent photon approximation”. The problem with the approximation is that the integral in eq. 3.39 diverges logarithmically. The approximation is only valid if we include a cutoff parameter q_t^{\max} , determined by the value of q_t at which $\sigma_{\gamma^*T}(Q, \omega)$ drops to zero. A hint to obtain this parameter is to look at figure 3.7. We see that the transverse virtual photon cross section drops to zero at $q_t \simeq \varepsilon$. Another hint comes from figure 3.9, where we plot the energy spectrum of the electron, $d\sigma/d\varepsilon$, for $\gamma = 3, 10,$ and $10,$ respectively, obtained from a numerical integration of eq. 3.32. We observe that the energy spectrum peaks at $\varepsilon \simeq 2 - 3$, irrespective of the value of γ . We thus conclude that an appropriate value of the cutoff parameter is $q_t^{\max} = 2$.

Inserting this value in eq. 3.39 we get

$$\frac{d\sigma}{d\varepsilon} = \frac{1}{\pi} \left(\frac{Z_T e}{v} \right)^2 \frac{1}{\omega} \sigma_\gamma(\omega) \left[\ln(4x + 1) - 4 \frac{x}{4x + 1} \right], \quad \text{where } x = \frac{\gamma^2 - 1}{\omega^2}. \quad (3.40)$$

The dotted curve shown in figure 3.5 is the integral of the above equation over ω . We see that this approximation is very reasonable, for large γ . It is only for the very extremely large γ 's that we obtain $\sigma = (2.86 \text{ pb}) Z_T^2 \ln \gamma$, where the number inside parenthesis comes from $(2\alpha/\pi) \int_2^\infty d\omega \sigma_\gamma(\omega) / \omega = 2.86 \text{ pb}$. Only at $\gamma \sim 10^3$, and larger, the approximation presented in ref. [10] becomes close (in the range of 10%) to the result obtained with the equation above.

Chapter 4

PRODUCTION OF EXOTIC ATOMS AT CERN LARGE HADRON COLLIDER

4.1 Production of exotic atoms in ion-ion collisions

From Chapter 3 we have

$$A_\mu(\mathbf{r}, t) = v_\mu \phi, \quad \text{with } v_\mu = (1, \mathbf{v}), \quad \text{and } \phi(\mathbf{r}, t) = \frac{\Gamma Z e^2}{|\mathbf{R} - \mathbf{R}'(t)|}, \quad (4.1)$$

where

$$\mathbf{r} = (x, y, z), \quad \mathbf{R} = (x, y, \Gamma z), \quad \mathbf{R}' = (b_x, b_y, \Gamma vt),$$

and \mathbf{v} is the relative velocity between the nuclei which we will take to lie along the z -axis. Γ is the relativistic Lorentz factor $\Gamma = 1/(1 - v^2)^{1/2}$ (unless otherwise explicitly stated, we use the units $\hbar = c = 1$).

Also from Chapter 3, the pair-production amplitude at time t for a collision with impact parameter $b = \sqrt{b_x^2 + b_y^2}$ is given in terms of the transition density $\rho(\mathbf{r})$ and the current density $\mathbf{j}(\mathbf{r})$, as

$$a_{1st}(\mathbf{p}, b, t) = \frac{1}{i} \int_{-\infty}^t dt' e^{i\omega t'} \int d^3r j_\mu(\mathbf{r}) A^\mu(\mathbf{r}, t'), \quad (4.2)$$

where $\omega = \epsilon + m - I$, with ϵ equal to the energy of the free positive particle and I being the ionization energy of the negative captured particle. m is the rest mass of either particle. The transition current is given in

terms of the Dirac matrices γ_μ , and the particle and anti-particle wave functions, i.e., $j_\mu(\mathbf{r}) = e\bar{\Psi}_-\gamma_\mu\Psi_+$, where Ψ_- is the wavefunction for the captured negative particle and Ψ_+ that of the free positive particle.

The multipole expansion of $j_\mu A^\mu$ has been extensively discussed in details in Refs. [20, 21, 22]. Replacing the Schrödinger by the Dirac currents in their results, one finds that $j_\mu(\mathbf{r})A^\mu(\mathbf{r}, t) = \sum_{\pi l \kappa} V_{\pi l \kappa}(\mathbf{r}, b, t)$, where $\pi = E, M$ and $l = 0, 1, 2, \dots$, and $\kappa = -l, \dots, l$ denote the multipolarities. For electric E1 (electric dipole) and E2 (electric quadrupole) multipolarities,

$$V_{E1\kappa}(\mathbf{r}, b, t) = \bar{\Psi}_-(\mathbf{r})(1 - \gamma_0\gamma_z)rY_{1\kappa}(\hat{\mathbf{r}})\Psi_+(\mathbf{r}) \times \frac{\Gamma Ze^2\sqrt{2\pi/3}}{(b^2 + \Gamma^2v^2t^2)^{3/2}} \begin{cases} \mp b, & (\text{if } \kappa = \pm 1) \\ \sqrt{2}vt & (\text{if } \kappa = 0), \end{cases} \quad (4.3)$$

$$V_{E2\kappa}(\mathbf{r}, b, t) = \bar{\Psi}_-(\mathbf{r})(1 - \gamma_0\gamma_z)r^2Y_{2\kappa}(\hat{\mathbf{r}})\Psi_+(\mathbf{r}) \times \frac{\Gamma Ze^2\sqrt{3\pi/10}}{(b^2 + \Gamma^2v^2t^2)^{5/2}} \begin{cases} b^2, & (\text{if } \kappa = \pm 2) \\ \mp(\Gamma^2 + 1)but, & (\text{if } \kappa = \pm 1) \\ \sqrt{2/3}(2\Gamma^2v^2t^2 - b^2) & (\text{if } \kappa = 0). \end{cases} \quad (4.4)$$

In addition, for magnetic dipole (M1) [22],

$$V_{M1\kappa}(\mathbf{r}, b, t) = \left(\frac{p_z}{m}\right)\bar{\Psi}_-(\mathbf{r})(1 - \gamma_0\gamma_z)\gamma_zrY_{1\kappa}(\hat{\mathbf{r}})\Psi_+(\mathbf{r}) \times \frac{\Gamma Ze^2\sqrt{2\pi/3}}{(b^2 + \Gamma^2v^2t^2)^{3/2}} \begin{cases} \pm b, & (\text{if } \kappa = \pm 1) \\ 0 & (\text{if } \kappa = 0). \end{cases} \quad (4.5)$$

For the positive particle wavefunction we use a plane wave and a correction term to account for the distortion due to the nuclear charge [7]. The wavefunction is given by $\Psi_+ = \mathcal{N} [v(\mathbf{p}) \exp(i\mathbf{p} \cdot \mathbf{r}) + \Psi'_+]$, where $\mathcal{N}(\epsilon) = \exp(\pi a_+/2) \Gamma(1 + ia_+)$, with $a_+ = Ze^2 m/p$, with \mathbf{p} being the proton momentum, $v(\mathbf{p})$ the particle spinor and $|\mathcal{N}(\epsilon)|^2 = 2\pi a_+ / [\exp(2\pi a_+) + 1]$. The correction term Ψ'_+ is given by eq. (B5) of ref. [7], which for our purposes can be written as

$$\Psi'_+(\mathbf{r}) = \frac{Ze^2}{2\pi^2} v(\mathbf{p}) \int d^3q e^{-i\mathbf{q} \cdot \mathbf{r}} \frac{2\gamma^0 \epsilon + i\boldsymbol{\gamma} \cdot (\mathbf{q} - \mathbf{p})}{(\mathbf{p} - \mathbf{q})^2 (q^2 - p^2)}, \quad (4.6)$$

with $\epsilon = \sqrt{p^2 + m^2}$. Parts of this integral can be done analytically.

For the negative particle we use the distorted hydrogenic wavefunction [7] for capture to the ground state,

$$\Psi_-(\mathbf{r}) = \frac{1}{\sqrt{\pi}} \left(\frac{Z}{a} \right)^{3/2} \left[1 - \frac{i}{2} \gamma^0 \boldsymbol{\gamma} \cdot \boldsymbol{\nabla} \right] u(\epsilon_0) \exp(-Zr/a), \quad (4.7)$$

where u is the negative particle spinor, ϵ_0 is the energy of the exotic atom bound-state, and $a = 1/me^2$ being the hydrogen Bohr radius. As noted in [7], the reason why we need to keep the corrections in the wavefunctions to first order in Ze^2 is because for $\epsilon \gg m$ these corrections yield a term of the same order of magnitude as the plane-wave to the total cross section. The reason for this are the small distances which enter in the calculation of the integral in Eq. (4.2). The wavefunc-

tion corrections are essential to account for the short distance effects properly. Such effects are not as important in the case of bound-free production of heavy particle-antiparticle pairs, but we keep them for a more accurate description of the process.

To gain insight into the pair production probability with capture and its distribution in space-time, we will compare our numerical results with simplified calculations which neglect the above mentioned short-distance corrections of the wavefunction of the captured negative particle as well as of the free positive particle. This is a reasonable approximation for small values of the free particle energy, i.e. for $\epsilon \sim m$, as we show later. This approximation allows us to obtain the coordinate integral in a_{1st} analytically, by using

$$\begin{aligned}
 F_{\lambda\kappa}(\mathbf{p}) &= \frac{1}{\sqrt{\pi}} \left(\frac{Z}{a}\right)^{3/2} \int d^3r e^{-i\mathbf{p}\cdot\mathbf{r}} r^\lambda Y_{\lambda\kappa}(\hat{\mathbf{r}}) e^{-Zr/a} \\
 &= 32\sqrt{\pi} \left(\frac{a}{Z}\right)^{5/2} \begin{cases} \frac{x_p}{(1+x_p^2)^3} Y_{1\kappa}(\hat{\mathbf{p}}) & \text{for } \lambda = 1, \\ -\frac{6(a/Z)x_p^2}{(1+x_p^2)^4} Y_{2\kappa}(\hat{\mathbf{p}}) & \text{for } \lambda = 2. \end{cases} \quad (4.8)
 \end{aligned}$$

where $x_p = ap/Z$ and $\hat{\mathbf{p}}$ is the unit vector for the positive particle momentum direction with respect to a z-axis pointing along the beam direction. To calculate total cross sections we keep the wavefunction corrections, Eqs. (4.6) and (4.7). In this case, some of the coordinate integrals need to be performed numerically.

The exotic atom production probability density, at time t and for a collision with impact parameter b , is obtained by the square of expression (4.2), i.e.,

$$\mathcal{P}(\mathbf{p}, b, t) = \sum_{\text{spins}} |a_{1st}(\mathbf{p}, b, t)|^2, \quad (4.9)$$

where the sum over spins is performed with standard trace techniques.

The production probability, at time t and for a collision with impact parameter b , is obtained by integration over momentum,

$$P(b, t) = \int \frac{d^3p}{(2\pi)^3} \mathcal{P}(\mathbf{p}, b, t). \quad (4.10)$$

If one neglects the derivative corrections in the particle and anti-particle wavefunction, the sum over spins in eq. (4.9) yields

$$P(b, t) = 4m \sum_{\lambda\kappa} \left| \int \frac{d^3p}{(2\pi)^3} \sqrt{\epsilon + m} \mathcal{N}(\epsilon) F_{\lambda\kappa}(\mathbf{p}) \right|^2 |G_{\lambda\kappa}(b, \omega, t)|^2, \quad (4.11)$$

where the small binding energy I was neglected as it is small compared to the mass m . The functions $G_{\lambda\kappa}$ are defined as $G_{\lambda\kappa} = \int_0^t \exp\{-i\omega t'\} \{\dots\}$, where the terms inside braces $\{\dots\}$ are the time-dependent terms to the right of the positive particle wavefunctions in eqs. (4.3-4.5). For the M1 magnetic multipole the same equation can be used with the replacement $\sqrt{\epsilon + m} \rightarrow \sqrt{\epsilon - m}$, and multiply it by an extra factor $(p_z/m)^2$.

The cross section for bound-free pair production is obtained by integrating the production probability over all impact parameters at $t = \infty$, i.e.,

$$\sigma = \int d^2b P(b, \infty). \quad (4.12)$$

The above integral over impact parameters diverge if the potentials of eqs. (4.3)-(4.5) are used. The reason is that these potentials are obtained from an expansion of the full Lienard-Wiechart potential of eq. (4.1) which is only valid for distant collisions, i.e., when the Lorentz-modified projectile coordinate R' is larger than the Lorentz-modified internal coordinate R . A better approach is to use a full representation of the potential in terms of a momentum transform, as done in ref. [7], i.e.,

$$\phi(\mathbf{r}, t) = \frac{\Gamma Z e}{2\pi^2} \int d^3q \frac{e^{i\mathbf{q} \cdot [\mathbf{R} - \mathbf{R}'(t)]}}{q^2}. \quad (4.13)$$

This introduces extra integrations over the virtual momentum \mathbf{q} increasing considerably the numerical effort [7].

Recently, it was shown that one can treat the effects of close collisions ($R' < R$) by using the potentials of eqs. (4.3-4.5) for $R' > R$ and the potentials for close collisions given by [22] (we will only treat

the E1 case for reasons to be shown later)

$$V_{E1\kappa}^{\text{close}}(\mathbf{r}, b, t) = \bar{\Psi}_-(\mathbf{r}) (1 - \gamma_0\gamma_z) \frac{1}{r^2} Y_{1\kappa}^*(\hat{\mathbf{r}}) \Psi_+(\mathbf{r}) Z e^2 \\ \times \sqrt{\frac{2\pi}{3}} \{g_0(\Gamma) + c_\kappa g_2(\Gamma)\} \begin{cases} \sqrt{2}vt & \text{if } \kappa = 0 \\ \mp b & \text{if } \kappa = \pm 1 \end{cases} \quad (4.14)$$

where $c_0 = 2/5$, $c_{\pm 1} = -1/5$, and

$$g_0(\Gamma) = \frac{1}{v^2} \ln[\Gamma(1+v)], \quad g_2(\Gamma) = \frac{5}{4v} \left(\frac{3}{v^2} - 1 \right) \ln[\Gamma(1+v)] - \frac{15}{2v^2}. \quad (4.15)$$

The integrals over \mathbf{r} now have to be carried out by using eq. (4.3) for $R' > R$ and eq. (4.14) for $R' < R$. In particular, for $b = 0$ one gets

$$\frac{1}{i} \int_{-\infty}^t dt' e^{i\omega t'} V_{E1\kappa}^{\text{close}}(\mathbf{r}, b, t') = \delta_{\kappa,0} \bar{\Psi}_n(\mathbf{r}) (1 - \gamma_0\gamma_z) \frac{1}{r^2} Y_{10}^*(\hat{\mathbf{r}}) \Psi_p(\mathbf{r}) \\ \times 4 \sqrt{\frac{\pi}{3}} Z e^2 \Gamma v \{g_0(\Gamma) + c_0 g_2(\Gamma)\} \\ \times \frac{1}{\omega^2} \begin{cases} \sin\left(\frac{R\omega}{\Gamma v}\right) - \frac{R\omega}{\Gamma v} \cos\left(\frac{R\omega}{\Gamma v}\right) & \text{if } R > R' \\ e^{-iR\omega/\Gamma v} \left(i - \frac{R\omega}{\Gamma v}\right) + i e^{it\omega} (it\omega - 1) & \text{if } R' > R \end{cases}$$

For $\Gamma \gg 1$, $g_0(\Gamma) + c_0 g_2(\Gamma) = 2 \ln(2\Gamma) - 15/2$. When $t = \infty$ only the upper term in the last part of this equation contributes ($R < \infty$) to the production probability.

We use the above separation of close and distant collisions to make an estimate of their relative contributions to the total cross section. To obtain the total cross sections we use the formalism developed

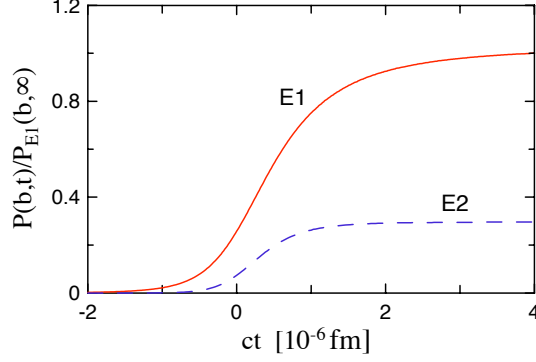


Figure 4.1: Relative probability $P_{E\lambda}(b, t)/P_{E1}(b, t = \infty)$, for production of a muonic atom in pp collisions at the LHC with an impact parameter $b = a_{muon} = 255$ fm, where a_{muon} is the Bohr radius for a muonic atom.

in ref. [7] which allows a better reduction of the integrations in momentum space. Adapting their results for ion-ion collisions, we get

$$\sigma = \frac{256\pi Z^7 e^4}{3a^5} \int_0^\infty d\epsilon |\mathcal{N}(\epsilon)|^2 \frac{p}{q} \times \int_0^\infty dq \frac{q(q^2 + \omega^2/\Gamma^2 v^2)^{m-I}}{(q^2 - \omega^2/\Gamma^2 v^2)^2} \frac{(p^2 + 3q^2 + 3\omega^2/v^2)(3p^2 + q^2 + \omega^2/v^2)}{(q^2 + \omega^2/v^2 - p^2)^6} \quad (4.17)$$

Notice that we keep the relative velocity v between the colliding nuclei in all formulas, although $v \sim c$. This is necessary because sometimes important combinations of 1 and v conspire and combine into Lorentz factors $\Gamma = (1 - v^2)^{-1/2}$ in subsequent steps of the calculations.

4.2 Results

At the Large Hadron Collider (LHC) at CERN the Lorentz gamma factor in the laboratory frame, Γ_{lab} , is 7000 for p-p, 3000 for Pb-Pb collisions. The relationship between the Lorentz contraction factor associated with the relative velocity between the colliding nuclei, and the

collider energy per nucleon, E/A , in GeV, is given by $\Gamma = 2(\Gamma_{lab}^2 - 1) \simeq 2(1.0735E/A)^2$. This means that for the production of exotic atoms we have effectively $\Gamma \simeq 10^8$ for p-p and $\Gamma \simeq 10^7$ for Pb-Pb collisions.

In figure 4.1 we plot the relative probability $P_{E\lambda}(b, t)/P_{E1}(b, t = \infty)$, for production of a muonic atom in pp collisions at the LHC with an impact parameter $b = a_{muon} = 255$ fm, where a_{muon} is the Bohr radius for a muonic atom. The time scale is in units of 10^{-8} fm/c. The probability is normalized so that it is equal to the asymptotic value of the E1 multipolarity. In absolute values the probabilities are very small, justifying the use of perturbation theory. The E2 probability tends to its asymptotic value faster than E1. This can be understood from Eqs. (4.3) and (4.4) as the time-dependence of the E2-field is determined by a higher inverse power of time. The asymptotic value of the E2 probability is about a factor 4 smaller than the E1 case. As a function of the impact parameter, the E2 probability decreases with an additional $1/b^2$ dependence, as compared to E1. This yields cross sections for pair-production with capture due to the E2 field being much smaller than that with E1. The probabilities and cross sections are also much smaller in the case of the M1 multipolarity, due to the factor (p_z/m) in Eq. 4.5. This is also substantiated by the approximation in Eq. (4.11), which has a factor $\sqrt{\epsilon - m}$ instead of the $\sqrt{\epsilon + m}$ which appears in the

electric multipole cases. For low positive particle momentum this leads to a further suppression of the M1 multipolarity.

We thus conclude that the E1 multipolarity alone is responsible for most part of the bound-free pair-production probability. This comes as no surprise because of the very large Γ factor in the frame of reference of the exotic atom. The spatial distribution of the time-dependent field is compressed as a pancake-like object with a spatial width $\Delta z = c\Delta t = b/\Gamma$. For $b = 200$ fm this is equal to $\Delta z \simeq 10^{-6}$ fm for the LHC. Even for very large impact parameters, e.g., $1\text{\AA} = 10^5$ fm, Δz is small compared to the nuclear sizes. The E2 field is a measure of the “tidal” force, proportional to the spatial spreading of the electric field [3]. This “tidal” effect becomes larger at smaller velocities, when the field lines are not as compressed. The large value of Γ also leads to a complete dominance of the $\kappa = \pm 1$ component of the E1 field in eq. (4.3).

The above discussion implies that in order to calculate pair-production with capture in ultra-peripheral collisions at the LHC once only needs to consider the E1 field, with $\kappa = \pm 1$, in eq. (4.3). The asymptotic production probability amplitude, Eq. (4.2), for a given impact parameter b , is then given by

$$a_{\kappa=\pm 1}(\mathbf{p}, b) = 2\kappa i \frac{Ze^2}{vb} \sqrt{\frac{2\pi}{3}} \xi K_1(\xi) \int d^3r \bar{\Psi}_n(\mathbf{r}) (1 - \gamma_0 \gamma_z) r Y_{1\kappa}(\hat{\mathbf{r}}) \Psi_p(\mathbf{r}), \quad (4.18)$$

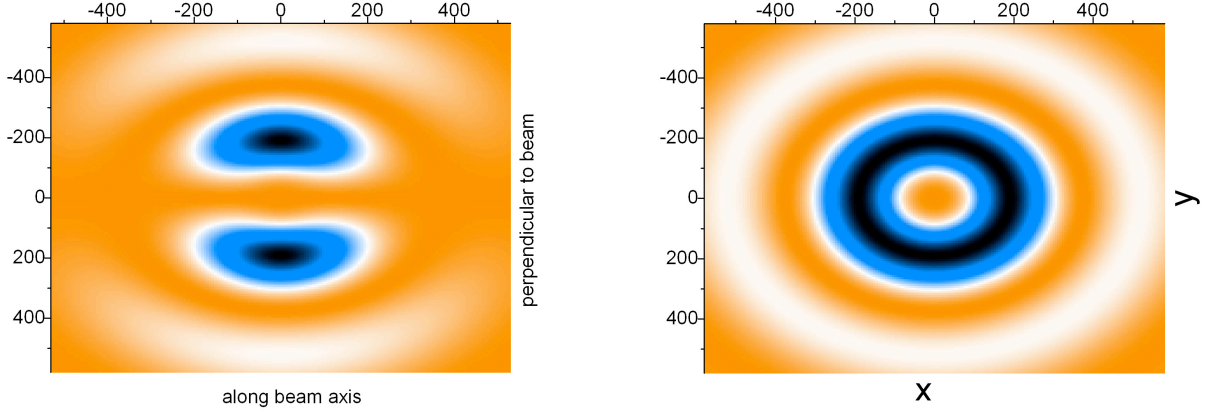


Figure 4.2: Left: Coordinate distribution in the plane along the beam axis of the probability for production of muonic atoms with capture in the K-shell with pp collisions at the LHC. The impact parameter is chosen as $b = a_{muon} = 255$ fm and is along the vertical axis. Right: Same as the previous figure, but in the plane perpendicular to the beam axis. The impact parameter vector lies along the x direction.

where $\xi = \omega b/\Gamma v$ and K_1 is the modified Bessel function of first order. Note that $\xi K_1(\xi) \simeq 1$ for $\xi \lesssim 1$. For $\xi > 1$, $\xi K_1(\xi)$ drops to zero exponentially. This means that the production probability drops as $1/b^2$ up to $b_{max} \approx \Gamma \hbar c/m \approx 10^{10}(\text{MeV}\cdot\text{fm})/mc^2$ for pp collisions at the LHC. For production of muons and pions with capture this means $b_{max} \approx 10^8$ fm, whereas for proton-antiproton with capture, this means $b_{max} \approx 10^7$ fm.

In the left panel of Fig. 4.2 we show the coordinate space distribution for production of muons with capture in the K-shell in pp collisions at the LHC. The distribution is shown in a plane containing the beam direction and the impact parameter vector. The calculation

is done for the E1 multipolarity and for an impact parameter $b = a_{muon}$. The positive muon energy is taken as $\epsilon = 1.1m_\mu$ and its direction of emission is chosen as 100° when measured along the direction of motion of the muonic atom. One notices that the production mechanism is more efficient in regions perpendicular to the beam axis. The darker areas are representative of larger production rates in coordinate space. The right figure shows the same result, but as seen in the plane perpendicular to the beam axis. In this case, the impact parameter vector lies along the x-direction. We observe that the probability density is largest within a torus-like region with a radius $r \approx a_{muon}$ from the origin of the muonic atom, with the torus axis along the beam direction.

We now use Eq. (4.16) to obtain the production probability of muonic atoms at the LHC at zero impact parameter. We find that the probability is 5 orders of magnitude smaller than that with $b = a_{muon}$. We easily understand this result by inspection of the equation (4.16). When $t = \infty$ only the upper term in the last part contributes ($R < \infty$) to the production probability. This term oscillates harmonically as a function of $\omega R/\Gamma v \approx 2mR/\Gamma v$. For R along the z-direction this variable varies as $2mc^2z/\hbar c$. As the largest contribution to the integral arises for $z \approx a_{muon}$, this variable is much larger than the unity, causing the harmonic functions to oscillate wildly, and leading to a small value of the integral over coordinates (matrix element).

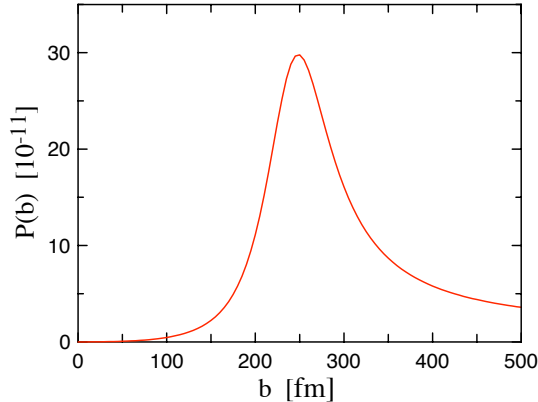


Figure 4.3: Probability of muonic atom production in pp collisions at the LHC as a function of the impact parameter.

We now perform an estimate of the contribution of collisions with small impact parameters by using Eq. (4.16) and integrating it numerically over time, space, and impact parameters, for several energies and angles of the emitted positive muon. To obtain these estimates, we have used the functions Ψ_- and Ψ_+ without the derivative corrections. The integrals are performed for $b < a_{muon}$. We compare with the results obtained using Eq. (4.18) for $b \geq a_{muon}$. We find that the impact parameter region $b > a_{muon}$ contributes at least a factor 100 more to the cross section than the region with $b < a_{muon}$. Such findings are confirmed by an integration over the free positive muon energy. This is also confirmed using Eqs. (4.18) and (4.16) and Ψ_- and Ψ_+ without derivative corrections. Our numerical results are shown in figure 4.3. We clearly see that the small impact parameters, $b \lesssim a_{muon}$ yield a much smaller probability than $b \gtrsim a_{muon}$.

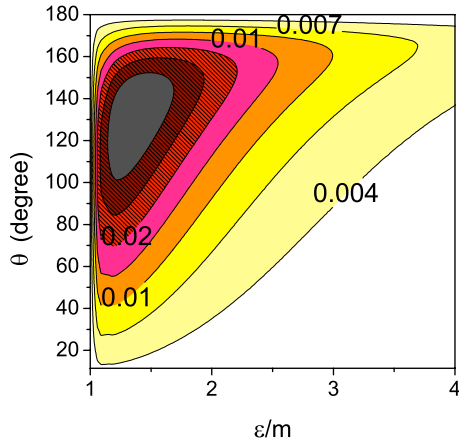


Figure 4.4: Contour plot with the angular distribution of the positive muon when the negative muon is captured by a proton at the LHC, as a function of the angle that the free muon has with the direction of motion of the muonic atom and of the energy of the free positive muon.

In Fig. 4.4, we plot the angular distribution of positive muon when the negative muon is captured by a proton at the LHC as a function of the angle that the free muon has with the direction of motion of the muonic atom and of the energy of the free positive muon. The impact parameter is chosen as $b = a_{muon}$. The units in the contour plot are arbitrary, with the darker areas being the region of highest probability. The plot shows that the higher the electron energy is, the more backward peaked the distribution becomes. In the frame of reference of the atom, the angular distribution of the positive particles is backward peaked, along the beam axis, opposite in the direction of motion of the nucleus capturing the muon. The higher the positive muon energy is, the more backward peaked the distribution becomes.

exotic atom	pp	Pb-Pb
hydrogenic	63.4 pb	132 b
muonic	44.8×10^{-4} pb	0.16 mb
pionic	21.3×10^{-4} pb	0.09 mb
kaonic	1.3×10^{-4} pb	4.3 μ b
ρ -atom	0.51×10^{-4} pb	1.3 μ b
protonium	0.09×10^{-4} pb	0.3 μ b

Table 4.1: Cross sections for production of exotic atoms in pp and Pb-Pb collisions at the CERN Large Hadron Collider (LHC).

The most probable energy of the free muon is non-relativistic, i.e., $\epsilon \simeq m$. For such low energy muons the opening angle for emission of the free muon is larger. In a collider, a Lorentz transformation of these results to the laboratory frame implies that all particles are seen along the beam direction, within an opening angle of order of $1/\Gamma$. That is, all positive particles are seen along the same direction as the beam.

Using Eq. (4.17) we calculate the cross sections for production of exotic atoms in pp and Pb-Pb collisions at the LHC. Our results are shown in Table I. Whereas the cross sections are small for pp collisions, they are by no means negligible for Pb-Pb collisions. This is due to the factor Z^7 in Eq. (4.17), although a reduction of this Z dependence arises from the distortion factor \mathcal{N} .

4.3 Conclusions

Because of the very strong electromagnetic fields of short duration, new and interesting physics arise at the LHC. We have studied the space-time dependence of the cross sections for production of exotic

atoms in ultraperipheral collisions at the LHC. We have considered the case of muonic, pionic and anti-protonic (or protonium) atoms. A very transparent and simple formulation is obtained using the lowest-order corrections for the positron and electron wavefunctions and a multipole expansion of the electromagnetic field separated in the regions of small (i.e., b smaller than the Bohr radius) and of large impact parameters. Whereas most of our discussion and conclusions have been based on calculations of muonic atoms, the qualitative aspects will not change for pionic, protonic, or other exotic atoms, except for the magnitude of the cross sections. The space-time and impact parameter dependences will also be similar for Pb-Pb collisions.

We considered the capture of negative particles in the K-shell of either the proton of the Pb nucleus. This is the largest contribution to the capture cross section. Inclusion of capture to all other shells will increase by about 20% of the our calculated cross sections, according to early estimates for electron-pair production with capture [3]. Depending on the relevance of this process to peripheral collisions with relativistic heavy ions and on the accuracy attained by the experiments, further theoretical studies on the capture to higher orbits could be necessary. The distortion of the wavefunctions due to the nuclear size should also be considered. Due to their small charges, pp collisions will not yield a measurable amount of exotic atoms, but in Pb-Pb col-

lisions we expect an abundant number of events of production of exotic atoms. This will open opportunities to study the properties of exotic atoms and their decay widths.

Bibliography

- [1] E. Papageorgiu, Phys. Rev. D 40, 92 (**1989**).
- [2] M. Grabiak, B.Müller, W. Greiner, G. Soff, and P. Koch, J. Phys. G 15, L25 (**1989**).
- [3] C.A. Bertulani and G. Baur, Phys. Rep. 163, 299 (**1988**).
- [4] C.A. Bertulani and G. Baur, Physics Today, March **1994**, p. 22.
- [5] G. Baur et al., Phys. Lett. B 368, 251 (**1996**).
- [6] G. Blanford, Phys. Rev. Lett. 80, 3037 (**1998**).
- [7] C.A. Bertulani and G. Baur, Phys. Rev. D58, 034005 (**1998**).
- [8] K. Alder and A. Winther, "Electromagnetic Excitation", North-Holland, **1975**
- [9] PS210 collaboration, W. Oelert, spokesperson; G. Baur et al., Phys. Lett. B368 (**1996**) 251
- [10] C.T. Munger, S.J. Brodsky, and I. Schmidt, Phys. Rev. D49 (**1994**) 3228
- [11] C.A. Bertulani and G. Baur, Phys. Rep. 163 (**1988**) 299; Nucl. Phys. A505 (**1989**) 835

- [12] A. Aste et al., Phys. Rev. A50 (**1994**) 3980
- [13] A.J. Baltz et al., Phys. Rev A48 (**1993**) 2002
- [14] G. Baur, Phys. Lett. B311 (**1993**) 343
- [15] V.B. Berestetskii, E.M. Lifshitz, and L.P. Pitaevskii, *Relativistic Quantum Field Theory, Part 1*, 2nd ed. (Pergamon, New York, **1979**)
- [16] M. Mandelkern, letter of intent/experiment E862, Fermilab, available at <http://fnphyx-www.fnal.gov/experiments/e862/e862.html>
- [17] W. Heitler, *The Quantum Theory of Radiation*, 3rd. ed. (Oxford, New York, (**1954**))
- [18] The eq. (33.16) of ref. [15] has a wrong sign in the last term. The correct result, originally due to Sauter [19], is presented in the book of Heitler [17]
- [19] F. Sauter, Ann. Physik 9 (1931) 217; *ibid.* 11 (**1931**) 454
- [20] C. A. Bertulani, C. M. Campbell, and T. Glasmacher, Comp. Phys. Comm. 152, 317 (**2003**).
- [21] H. Esbensen and C. A. Bertulani, Phys. Rev. C 65, 024605 (**2002**).
- [22] K. Ogata and C. A. Bertulani, Prog. Theo. Phys. 121, 1399 (**2009**); Prog. Theo. Phys., in press.

[23] U. Becker, J. Phys. B20 (1987) 6563

Appendix A

POSITRON WAVEFUNCTION

Here we deduce a first order ($Z\alpha$) correction of the positron wavefunction, important in the calculation of the \overline{H} production cross section. To be general, we consider the production of a bound positron in a relativistic antinucleus, with charge $-Z$, incident on a target nucleus with charge Z_T . Much of our calculation is based on arguments presented in ref. [15] with connection to the photoelectric effect.

The Dirac equation for a positron in the field of the antinucleus is:

$$\varepsilon\Psi = [\vec{\alpha}\cdot(\mathbf{p} + e\mathbf{A}) - \beta m - e\phi] \Psi . \quad (\text{A.1})$$

For $\mathbf{A} = 0$:

$$\left[\varepsilon - U + \beta m + i\vec{\alpha}\cdot\vec{\nabla} \right] \Psi = 0 , \quad (\text{A.2})$$

where $U = -e\phi = -Ze^2/r$ is the Coulomb field. The positron will be most likely be produced at the s-state of the antinucleus. To lowest order the wavefunction is given by the non-relativistic hydrogenic wavefunction

$$\Psi_{non-r}(r) = \frac{1}{\sqrt{\pi}} \left(\frac{1}{a_0} \right)^{3/2} e^{-r/a_0}, \quad (\text{A.3})$$

where $a_0 = 1/(Ze^2m)$. To first-order, a corrected wavefunction (to order Ze^2) is given by

$$\Psi = v\Psi_{non-r} + \Psi^{(1)}, \quad (\text{A.4})$$

where v denotes the positron spinor.

Applying the operator $\varepsilon - U - m\beta + i\vec{\alpha} \cdot \vec{\nabla}$ to (A.2) we get

$$(\nabla^2 + p^2 - 2\varepsilon U) \Psi = \left(i\vec{\alpha} \cdot \vec{\nabla} U - U^2 \right) \Psi. \quad (\text{A.5})$$

Substituting (A.4) into (A.5) and expanding:

$$\begin{aligned} & (\nabla^2 + p^2 - 2\varepsilon U) \Psi_{non-r}v + (\nabla^2 + p^2 - 2\varepsilon U) \Psi^{(1)} \\ &= \left(i\vec{\alpha} \cdot \vec{\nabla} U - U^2 \right) \Psi_{non-r}v + \left(i\vec{\alpha} \cdot \vec{\nabla} U - U^2 \right) \Psi^{(1)}. \end{aligned} \quad (\text{A.6})$$

Since $p^2 = \varepsilon^2 + m^2 \simeq -2m|\varepsilon_s|$, $\Psi^{(1)} \propto Ze^2$, and $U \propto Ze^2$, we get to lowest order

$$(\nabla^2 + p^2 - 2\varepsilon U) \Psi_{non-r} \simeq (\nabla^2 - 2m|\varepsilon_s| - 2|\varepsilon_s|U) \Psi_{non-r} \simeq 0$$

and eq. (A.6) becomes

$$(\nabla^2 - 2m|\varepsilon_s| - 2mU)\Psi^{(1)} = \left(i\vec{\alpha} \cdot \vec{\nabla} U\right) \Psi_{non-r} v ,$$

or

$$\left(\frac{\nabla^2}{2m} - |\varepsilon_s| - \frac{Ze^2}{r}\right)\Psi^{(1)} = -\frac{i\vec{\alpha}}{2m} \cdot \left(\vec{\nabla} \frac{Ze^2}{r}\right) \Psi_{non-r} v \quad (\text{A.7})$$

The non-relativistic wave function obeys the equation

$$(\nabla^2/2m - |\varepsilon_s| + Ze^2/r)\Psi_{non-r} = 0$$

from which we deduce that

$$\left(\frac{\nabla^2}{2m} - |\varepsilon_s| - \frac{Ze^2}{r}\right)\vec{\nabla}\Psi_{non-r} = -\left(\vec{\nabla} \frac{Ze^2}{r}\right) \Psi_{non-r} \quad (\text{A.8})$$

Thus, if $\Psi^{(1)} = i/(2m)v\vec{\alpha} \cdot \vec{\nabla}\Psi_{non-r}$, it will be the solution of (A.7). An approximate solution of (A.1) is therefore

$$\Psi^{(+)} = \left[1 + \frac{i\vec{\alpha}}{2m} \cdot \vec{\nabla}\right] v\Psi_{non-r} = \left[1 + \frac{i}{2m} \gamma^0 \vec{\gamma} \cdot \vec{\nabla}\right] v\Psi_{non-r} , \quad (\text{A.9})$$

The relevant distances for the non-relativistic wavefunction are $r \sim 1/(mZe^2)$. The correction term should be good within these distances. But, for the ground state (or any s-state) it can be used for any value of r , since the derivative of the exponential function (A.3) is always proportional to Ze^2 . Because of that, we can use the corrected wavefunction in our calculation of \overline{H} production where, as we see in

section 2, the small values of r are essential in the computation of the matrix elements.

Appendix B

ELECTRON WAVEFUNCTION

For the electron wavefunction we use a plane wave and a correction term to account for the distortion due to the antinucleus charge. As in Appendix A, the correction term is considered to be proportional to Ze^2 . The wavefunction is then given by

$$\Psi = u e^{i\mathbf{p}\cdot\mathbf{r}} + \Psi' . \quad (\text{B.1})$$

Only the Fourier transform of Ψ' will enter the calculation. This Fourier transform can be deduced directly from the Dirac equation for the electron in the presence of a Coulomb field of an antinucleus

$$\left(\gamma^0 \varepsilon + i \vec{\gamma} \cdot \vec{\nabla} - m \right) \Psi' = \frac{Ze^2}{r} \gamma^0 u e^{i\mathbf{p}\cdot\mathbf{r}} , \quad (\text{B.2})$$

Applying on both sides of this equation the operator $\left(\gamma^0 \varepsilon + i \vec{\gamma} \cdot \vec{\nabla} + m \right)$ we get

$$(\Delta + p^2) \Psi' = Ze^2 \left(\gamma^0 \varepsilon + i \vec{\gamma} \cdot \vec{\nabla} + m \right) (\gamma^0 u) \frac{e^{i\mathbf{p}\cdot\mathbf{r}}}{r} . \quad (\text{B.3})$$

Multiplying by $e^{-i\mathbf{q}\cdot\mathbf{r}}$ and integrating over d^3r we get

$$(p^2 - q^2) \Psi'_{\mathbf{q}} = Ze^2 [2\gamma^0 \varepsilon + i \vec{\gamma} \cdot (\mathbf{q} - \mathbf{p})] (\gamma^0 u) \frac{4\pi}{(\mathbf{q} - \mathbf{p})^2} , \quad (\text{B.4})$$

where we have used the identity $(\gamma^0 \varepsilon + i \vec{\gamma} \cdot \vec{\nabla} - m)(\gamma^0 u) = 0$. Thus,

$$\Psi'_{\mathbf{q}} \equiv (\Psi'_{\mathbf{q}})^* \gamma^0 = -4\pi Z e^2 \bar{u} \frac{2\gamma^0 \varepsilon + i \vec{\gamma} \cdot (\mathbf{q} - \mathbf{p})}{(\mathbf{q} - \mathbf{p})^2 (q^2 - p^2)} \quad (\text{B.5})$$

AppendixC

PLANE-WAVE BORN APPROXIMATION

In the plane wave Born approximation the transition matrix element is given by

$$T_{fi} = \int d^3r [\rho_{fi}(\mathbf{r}) \phi(\mathbf{r}) - \mathbf{j}_{fi}(\mathbf{r}) \cdot \mathbf{A}(\mathbf{r})] \quad (\text{C.1})$$

where

$$\begin{Bmatrix} \phi(\mathbf{r}) \\ \mathbf{A}(\mathbf{r}) \end{Bmatrix} = \begin{Bmatrix} 1 \\ \mathbf{v} \end{Bmatrix} \int d^3r' \frac{e^{i\omega|\mathbf{r}-\mathbf{r}'|}}{|\mathbf{r}-\mathbf{r}'|} \langle \mathbf{k}_f | \mathbf{r}' \rangle \langle \mathbf{r}' | \mathbf{k}_i \rangle, \quad (\text{C.2})$$

and $\langle \mathbf{k} | \mathbf{r} \rangle = e^{i\mathbf{k} \cdot \mathbf{r}}$ is a plane wave for the antiproton. Using

$$\frac{e^{i\omega|\mathbf{r}-\mathbf{r}'|}}{|\mathbf{r}-\mathbf{r}'|} = \frac{1}{2\pi^2} \int d^3K \frac{e^{i\mathbf{K} \cdot (\mathbf{r}-\mathbf{r}')}}{K^2 - \omega^2} \quad (\text{C.3})$$

and $\mathbf{J}_{fi} = \mathbf{v} \rho_{fi}$, we get

$$T_{fi} = 4\pi \int d^3r \frac{e^{i\mathbf{Q} \cdot \mathbf{r}}}{Q^2 - \omega^2} [\rho_{fi}(\mathbf{r}) - \mathbf{j}_{fi}(\mathbf{r}) \cdot \mathbf{v}] = 4\pi Z e \frac{F(\mathbf{Q})}{Q^2 - \omega^2}, \quad (\text{C.4})$$

where $\mathbf{Q} = \mathbf{k}_i - \mathbf{k}_f$ and $F(\mathbf{Q})$ is given by eq. (2.6). The cross section is given by

$$\frac{d\sigma}{d\Omega} = \left(\frac{E}{2\pi} \right)^2 \sum_{spins} \int |T_{fi}|^2.$$

For relativistic antiproton energies

$$\begin{aligned} Q_L &= k_i - k_f \cos \theta \simeq k_i - k_f \simeq \omega/v \\ Q_T &\equiv q_t = k_f \sin(\theta) \simeq Ev \sin(\theta) \quad \implies \quad d\Omega = d^2q_t / (Ev)^2 \end{aligned} \quad (\text{C.5})$$

so that

$$\sigma = 4 \left(\frac{Z_T e}{v} \right)^2 \sum_{spins} \int d^2q_t \frac{|F(\mathbf{Q})|^2}{(Q^2 - \omega^2)^2}. \quad (\text{C.6})$$

The q_t integration ranges from 0 to a maximum value Ev , where E and v are the antiproton energy and velocity, respectively. This value is however much larger than the relevant energies entering the matrix elements in $F(\mathbf{Q})$. Thus, the expression above is the same as the one derived in section 2, eq. (2.7).

VITA

Mark Allen Ellermann II was born in Brenham, Texas, on May 19, 1986, the son of Mark Allen Ellermann and Lisa Lanette Ellermann. After graduating from Mount Pleasant High School, Mount Pleasant, Texas, in 2004, he enrolled at Texas A&M University-Commerce at Commerce, Texas. He received the Bachelor of Science degree with a double major in physics and mathematics in May 2008 from Texas A&M University-Commerce. He was enrolled in the Graduate School of Texas A&M University-Commerce in August of 2008 and was awarded the Master of Science degree in December of 2010.

Permanent address: 4421 82nd Street Apt. 140
Lubbock, Texas 79424

